Report NAG5-859

THE ABSOLUTE RADIOMETRIC CALIBRATION OF THE ADVANCED VERY HIGH RESOLUTION RADIOMETER

P. N. Slater, P. M. Teillet, and Y. Ding
Optical Sciences Center
University of Arizona
Tucson, Arizona 85721

2 June 1989

Final Report for the period of 28 February 1988 to 29 February 1989

Prepared for
NATIONAL AERONAUTICS AND SPACE ADMINISTRATION
Goddard Space Flight Center
Greenbelt, Maryland 20771

TABLE OF CONTENTS

APPENDICES

ABSTRACT

This is the final report for NASA Grant NAG5-859, titled "The Absolute Radiometric Calibration of the Advanced Very High Resolution Radiometer." Three publications supported in part by the grant are included as appendices.

The measurement conditions are described for an intensive field campaign at White Sands Missile Range in November 1988 for the calibration of the AVHRRs on NOAA-9, NOAA-10 and NOAA-11, Landsat-4 TM, and SPOT. Three different methods for calibration of AVHRRs by reference to a ground surface site are reported, and results from these methods are compared.

Significant degradations in NOAA-9 and NOAA-10 AVHRR responsivities have occurred since prelaunch calibrations were completed. As of February 1988, degradations in NOAA-9 AVHRR responsivity were on the order of 37 percent in channel 1 and 41 percent in channel 2, and for the NOAA-10 AVHRR these degradations were 42 and 59 percent in channels 1 and 2, respectively. A continuing analysis of additional data is required for further characterization and update of these degradations in performance.

I. INTRODUCTION

This is the final report for NASA Grant NAG5-859, completed in February 1989.

We completed an intensive field campaign at White Sands Missile Range (WSMR) in November 1988, during which data were collected for the calibration of the AVHRRs on NOAA-9, NOAA-10 and NOAA-11, Landsat-4 TM, and SPOT. Originally, we planned to calibrate the NOAA AVHRRs with respect to the Landsat-4 TM. This has been impossible, because the necessary Landsat data from EOSAT have been unavailable. From December 1988 through February 1989 we were promised repeatedly that the data would be processed for us. It appears that until funding difficulties experienced by EOSAT are resolved, we will not receive this data. In March 1989 we contacted CNES and were told we could use SPOT calibration data to perform the intercalibration. We have since received the necessary data and are proceeding with the calibration. We expect to complete this task by mid-summer 1989.

A proposal for the continuation of AVHRR calibration is now in draft form. A joint proposal with John Barker (GSFC), it is titled "Retrospective and Current Radiometric Characterization/ Calibration of TM and AVHRR -- Lessons for EOS."

In the following sections we summarize the measurement conditions at WSMR during our November 1988 campaign. We offer general conclusions regarding our work to date on the calibration of NOAA-9 and NOAA-10, and include a summary of the limitations and sensitivities of the three calibration methods used. The report concludes with three appendices, each a publication supported by this grant, in which the different calibration methods are presented. The first is a 1988 paper by Teillet et al. titled "Absolute radiometric calibration of the NOAA AVHRR sensors;" the second is a 1988 paper by Biggar et al. titled "Laboratory calibration of field reflectance panels;" and the third is a 1988 paper by Slater titled "Radiometric calibration requirements and atmospheric correction."

The authors wish to thank the following persons for their contributions to this work:

Richard J. Bartell, Stuart F. Biggar, David I. Gellman, Mark W. Smith and Benfan Yuan of the Remote Sensing Group at the Optical Sciences Center; Ray D. Jackson and M. Susan Moran of the U.S. Department of Agriculture; Richard P. Santer of the University of Lille; and Brian L. Markham of the Goddard Space Flight Center.

II. WHITE SANDS MEASUREMENTS TAKEN IN NOVEMBER 1988

The measurements described below were taken on clear observation days during the WSMR field campaign, November 16-22, 1988.

1. GROUND MEASUREMENTS

a. Nadir reflectance factor measurements were taken over TM and SPOT sites with a Barnes MMR and an Exotech radiometer with TM or SPOT filters as appropriate. Data were collected also over two smaller areas, near Northrup strip, for different gypsum moisture levels. A Spectralon 610x610-mm panel was used as reference.

b. BRF measurements were taken with an Exotech radiometer over +/-45° to nadir with scan plane geometry appropriate to SPOT and AVHRR image acquisition.

c. Diffuse to global irradiance ratio data were collected with a Barnes modular multispectral radiometer (MMR) for determining the complex refractive index of aerosols.

2. ATMOSPHERIC AND METEOROLOGICAL DATA

a. Solar radiometer data were collected with an autotracker operating in 12 narrow spectral bands and with two manual Reagan instruments operating in 10 narrow spectral bands.

b. Meteorological data, i.e., barometric pressure, temperature, relative humidity and pyranometer data, were recorded continuously.

c. All-sky color photography was acquired at roughly 10-minute intervals during the day and more frequently around overpass time.

3. GROUND RADIANCE DETERMINATION FROM HELICOPTER

From a helicopter operating at 3,000 meters above sea level, ground radiances over the TM and SPOT sites were determined. An Exotech radiometer with SPOT or TM filters as appropriate, a Spectron radiometer and a video camera, boresighted on a rifle stock, were used for this purpose.

The satellite parameters of interest for the period of the campaign are listed in Table 1. The schedule of measurements, with brief pre- and post-calibration comments, is presented in Table 2. Figures 1 through 4 show the total integrated irradiance measured at WSMR for November 16 through 18 and November 21, 1988, with markers to show the NOAA-9, -10 and -11, TM, and SPOT image acquisition times. These four curves reflect the superb visibility conditions we enjoyed during those critical days of the campaign.

TABLE 1. Satellite Parameters of Interest

Date	Satellite	Overpass CUT	Look angles Nadir	AZ	Solar zenith
16 November	Landsat 4	17:08	1°	327°	53.5°
	SPOT	17:54	5°	119°	57.3°
	NOAA-9	23:10	28.30°	268°	80.9°
17 November	NOAA-9	23:00	12°	273°	79.1°
18 November	NOAA-10	15:24	32°	277°	71.9°
	NOAA-11	20:44	34°	260°	58.9°
	NOAA-9	22:48	8°	88°	77.1°
19 November	NOAA-10	15:01	5°	97°	75.9°
	NOAA-11	20:34	20°	260°	58.1°
	NOAA-9	22:37	27°	72°	75.3°
20 November	NOAA-10	14:40	39°	100°	79.8°
	NOAA-11	20:24	3°	275°	57.3°
	NOAA-9	22:26	41°	71°	73.6°
21 November	SPOT	17:59	1°	308°	54.5°
	NOAA-11	20:14	14°	98°	56.6°
22 November	SPOT	17:40	31°	100°	55.9°
	NOAA-11	20:04	30°	90°	56.0°

TABLE 2. November, 1988 WSMR Calibration Campaign

Date	Pre-Calibration Comments	Post-Calibration Comments
16 November	Solar data all day. Ground and heli. rad. data (1630-1830 hrs.) in AM only, BRF in PM only. Herman measurements at sundown.*	Good day. Very high visibility for all overpasses. Helicopter data for Landsat not possible, for SPOT was not timed therefore no good. All instruments appeared to work satisfactorily.**
17 November	Murphy/Toll meeting AM. BRF, small area reflectance and solar in PM only. Herman measurements at sundown.	Good visibility during overpass. All instruments appeared to work satisfactorily.
18 November	BRF at different azimuths; solar all day and small area reflectance as needed during day. Herman measurements repeated as necessary.	Thin cirrus during AM. Dust on horizon. All instruments appeared to work satisfactorily.**
19 November	BRF at different azimuths; solar all day and small area reflectance as needed during day. Herman measurements repeated as necessary.	Equipment calibration. No data taken, but NOAA-9 image could be good.
20 November	BRF at different azimuths; solar all day and small area reflectance as needed during day. Herman meaurements repeated as necessary.	Poor visibility. No data taken.
21 November	Solar all day. Heli AM (1730-1830 hrs.). BRF PM. Leave if one SPOT cal satisfactory or weather bad for 22 November.	Good visibility. Data taken during both overpasses. Helicopter video data look very good. Herman data in morning. Left site after NOAA-11 cal. All instruments appeared to work satisfactorily.**
22 November	Solar, BRF ground rad., no heli. Leave after SPOT cal.	No data collected--had returned home.

* These measurements are to attempt to validate a new spherical atmosphere radiative transfer code of B.M. Herman.

** The earlier model Reagan solar radiometer gave inconsistent results during the cold morning hours. The autotracker and later model Reagan radiometers appeared to give very consistent results.

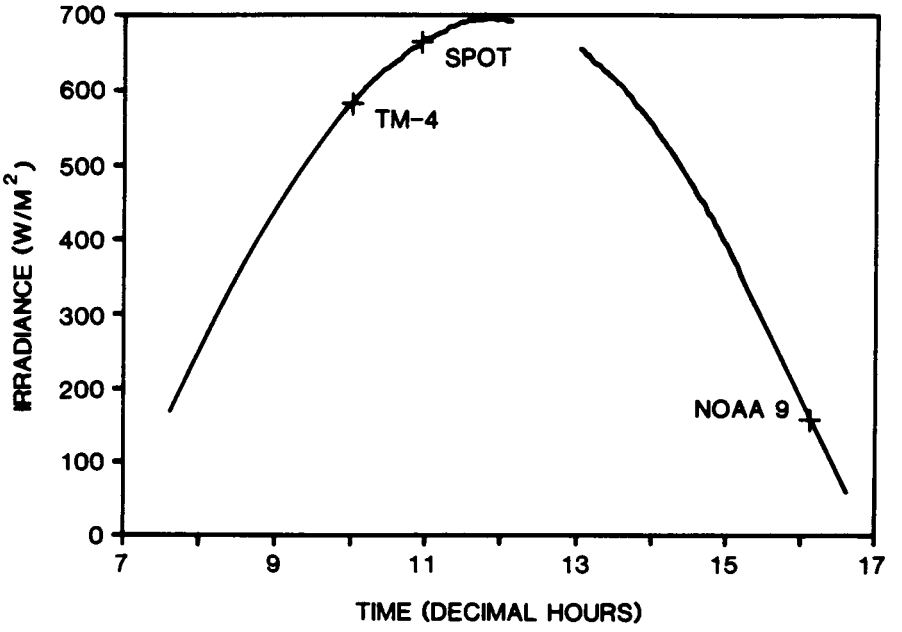

Figure 1. Total integrated irradiance, WSMR, 16 November 1988.

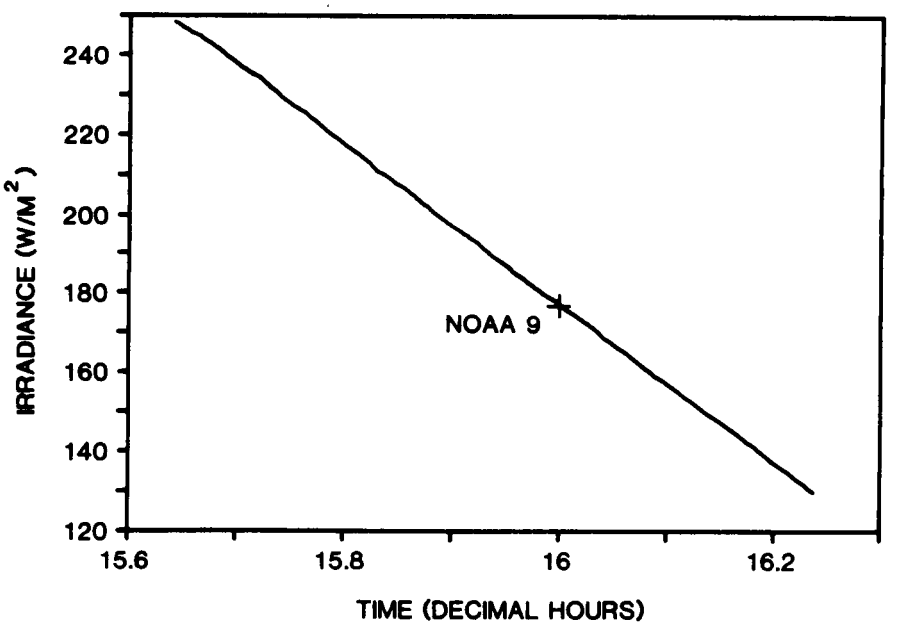

Figure 2. Total integrated irradiance, WSMR, 17 November 1988.

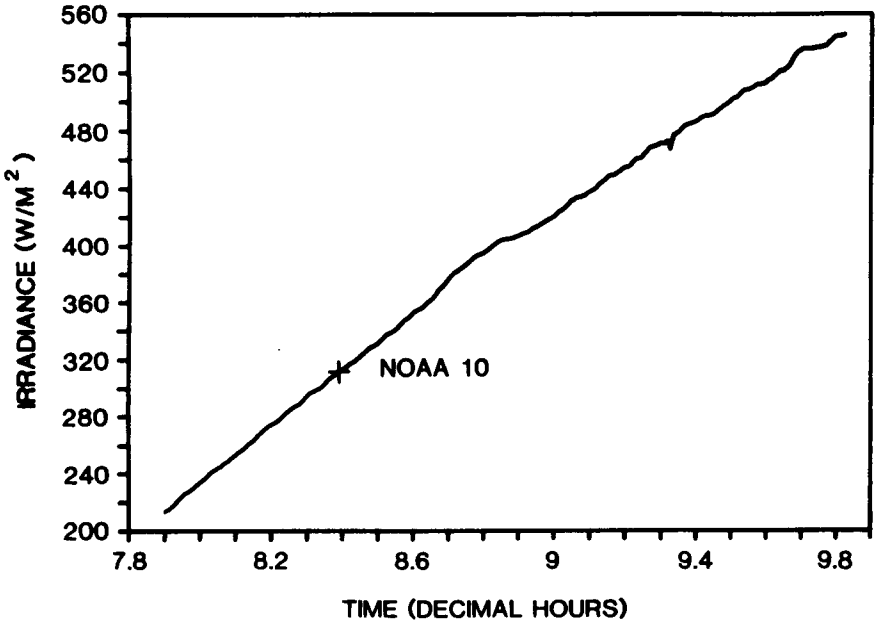

Figure 3. Total integrated irradiance, WSMR, 18 November 1988.

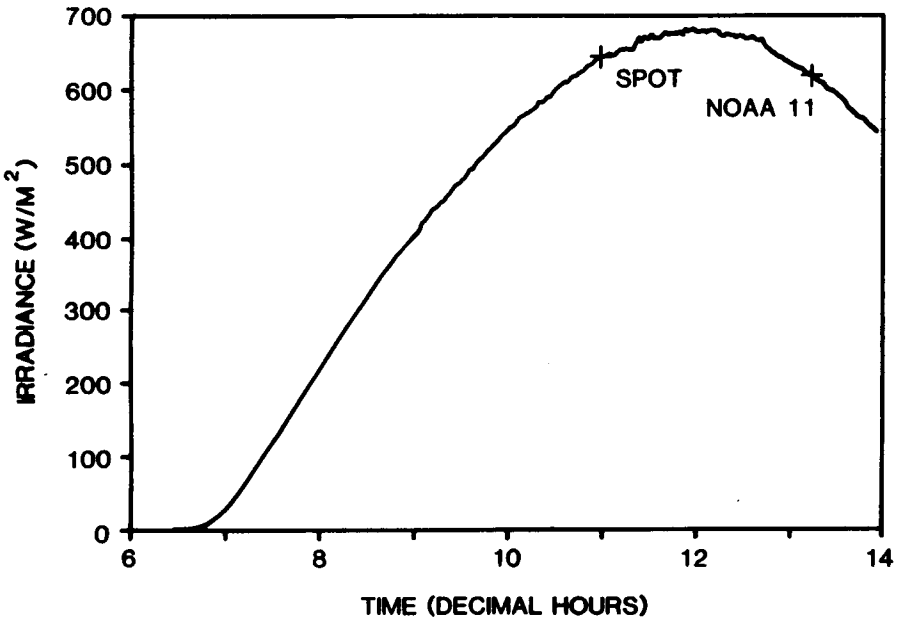

Figure 4. Total integrated irradiance, WSMR, 21 November 1988.

III. CONCLUSIONS

Significant degradations in NOAA-9 and NOAA-10 AVHRR responsivities have occurred since completion of the prelaunch calibration. As of February 1988, these degradations for the NOAA-9 instrument have been on the order of 37 percent in channel 1 and 41 percent in channel 2, and for the NOAA-10 AVHRR these degradations have been on the order of 42 and 59 percent in channels 1 and 2, respectively. A continuing analysis of additional data is required for further characterization and update of these degradations in performance.

There are some limitations to the use of Method 2 at the Rogers Lake site (a dry lake) at Edwards Air Force Base (see Appendix 1). The uniform area is limited to one AVHRR pixel (for nadir view angles less than 35 degrees relative to vertical at ground level) and is surrounded by terrain of much brighter and much darker reflectance on either side. In addition, in contrast to White Sands Missile Range, this site's surface is not very lambertian, therefore accurate BDRF corrections are important. It should be noted that the radiative transfer codes used assume lambertian reflectance. Using Method 2 at the Rogers Lake site, one is not likely to be able to track gain changes of less than 10 percent.

With Methods 1 and 3 (see Appendix 1), corrections for sun angle, view angle, and spectral differences between the higher resolution data and the AVHRR data are important, as is a good calibration of the high resolution sensor. For the data sets analyzed to date, the alkali-flats area at White Sands has proven suitable for both Method 1 and Method 3 approaches.

With Method 3, results generally are within 1 to 3 percent of results obtained with Method 1, under conditions usually expected at White Sands. Method 3 is not very sensitive to the assumed visibility and hence is not sensitive to aerosol optical depth. This method does, however, show some sensitivity to the assumed atmospheric profile and hence to water vapor, especially in channel 2.

Nevertheless, results for Method 3, which requires no field measurements and makes use of a simplified atmospheric model, are very promising. Because these results compare favorably with those from the more detailed methods, and because the method is not *overly* sensitive to assumed atmospheric conditions, the implication is that a reasonable calibration of satellite sensors may be possible by transfer, without the necessity of taking ground-based measurements. In this way, it would be relatively straightforward to monitor occasionally (and retrospectively as well) the status of AVHRR sensor radiometric responses.

APPENDIX 1.

Reprinted from SPIE Vol. 924—Recent Advances in Sensors, Radiometry, and Data Processing for Remote Sensing

Absolute radiometric calibration of the NOAA AVHRR sensors

P. M. Teillet,[1*] P. N. Slater,[1] Y. Mao,[1] Y. Ding,[1] B. Yuan,[1] R. J. Bartell,[1] S. F. Biggar,[1]
R. P. Santer,[1+] R. D. Jackson,[2] and M. S. Moran.[2]

1. Optical Sciences Center, University of Arizona, Tucson, Arizona, U.S.A. 85721.
2. U.S. Department of Agriculture, U.S. Water Conservation Laboratory, Phoenix, Arizona, U.S.A. 85040.
* On leave from the Canada Centre for Remote Sensing, Ottawa, Ontario, Canada K1A 0Y7.
+ On leave from the Laboratoire d'Optique Atmosphérique, Université des Sciences et Techniques de Lille, 59655 Villeneuve d'Ascq Cédex, France.

ABSTRACT

Three different approaches are described for the absolute radiometric calibration of the two reflective channels of the NOAA AVHRR sensors. Method 1 relies on field measurements and refers to another calibrated satellite sensor that acquired high-resolution imagery on the same day as the AVHRR overpass. Method 2 makes no reference to another sensor and is essentially an extension of the reflectance-based calibration method developed at White Sands for the in-orbit calibration of Landsat TM and SPOT HRV data. Method 3 achieves a calibration by reference to another satellite sensor, but it differs significantly from the first approach in that no ground reflectance and atmospheric measurements are needed on overpass day. Calibration results have been obtained using these methods for four NOAA-9 AVHRR images and for one NOAA-10 AVHRR image. A significant degradation in NOAA-9 AVHRR responsivity has occurred since the prelaunch calibration and with time since launch. The responsivity of the NOAA-10 AVHRR has also degraded significantly compared to the prelaunch calibration. The suitabilities of using Method 2 with the Rogers Dry Lake site in California and using Methods 1 and 3 at White Sands are discussed. The results for Method 3, which requires no field measurements and makes use of a simplified atmospheric model, are very promising, implying that a reasonable calibration of satellite sensors may be relatively straightforward.

1. INTRODUCTION

An increasing number of remote sensing investigations require radiometrically calibrated imagery from NOAA Advanced Very High Resolution Radiometer (AVHRR) sensors. Although a prelaunch calibration was done for these sensors, there is no proper capability for monitoring any changes in the in-flight absolute calibration for the visible and near infrared spectral channels. Hence, the possibility of using the reflectance-based method[1] developed at White Sands for in-orbit calibration of Landsat Thematic Mapper (TM) and SPOT Haute Resolution Visible (HRV) data to calibrate the AVHRR sensor has been under investigation. Three different approaches have been considered.

1.1 Method 1: Ground and atmospheric measurements and reference to another calibrated satellite sensor (Figure 1).

Ground-based reflectance measurements can be made over terrain areas corresponding to numerous Landsat TM or HRV pixels, but such measurements become impractical for the calibration of the AVHRR image data with pixel dimensions of 1.1 km by 1.1 km or greater. An alternative is to acquire AVHRR imagery of White Sands on the same day that a TM or HRV calibration has been carried out on the basis of ground reflectance factor and atmospheric measurements at Chuck Site in the alkali-flat region of White Sands. The methodology then takes advantage of the accurate calibration results for TM bands 3 and 4 or HRV bands 2 and 3 to effect a calibration of AVHRR channels 1 and 2. More specifically, a relatively uniform area corresponding to one or more AVHRR pixels is selected in the alkali-flat region and average digital counts are extracted for these AVHRR pixels and for pixels from the matching area in the TM or HRV imagery. With the help of radiative transfer computations and bidirectional reflectance data for the gypsum surface at White Sands, radiance at the entrance aperture of the AVHRR sensor is predicted. The

analysis takes into account differences in spectral response, sun angle, and viewing geometry between the TM or HRV and AVHRR data acquisitions.

1.2 Method 2: Ground and atmospheric measurements with no reference to another sensor (Figure 2).

The second approach is more closely analogous to the original reflectance-based approach used at White Sands to calibrate the TM or HRV sensors. It is based on detailed ground and atmospheric measurements near the time of AVHRR overpass, but it necessarily assumes the reflectance values to be representative of the whole pixel since these ground measurements can only encompass a portion of one AVHRR pixel. The availability of aircraft data can assist in the selection of an appropriately uniform area for this purpose. Although this method is not likely to be as accurate as the first, it has the distinct advantage of not requiring nearly coincident data acquisition from two different sensors.

1.3 Method 3: No ground and atmospheric measurements but reference to another sensor (Figure 3).

As with the first method, this approach achieves a calibration of the first two AVHRR channels by reference to another satellite sensor such as the TM or HRV on the same day. However, it differs significantly in that no ground and atmospheric measurements on the overpass day are needed. Instead, a standard data set of atmospheric conditions is used to approximate the actual atmosphere and historical bidirectional reflectance data are used to adjust for differences in illumination and viewing geometries. The same atmospheric parameters are adopted to estimate surface reflectance from the TM or HRV imagery and then to predict radiance at the AVHRR sensor from that surface reflectance (suitably adjusted for bidirectional effects and spectral bandpass differences). Because of this two-way use of the atmospheric model, errors introduced in one direction will be compensated to some extent in the reverse direction so that reasonable calibration results may be obtained if the procedure is not overly sensitive to the choice of atmospheric model. If it proves to be viable, this approach will be a valuable one because it will facilitate in-orbit sensor calibration without the complexity and expense of field measurements.

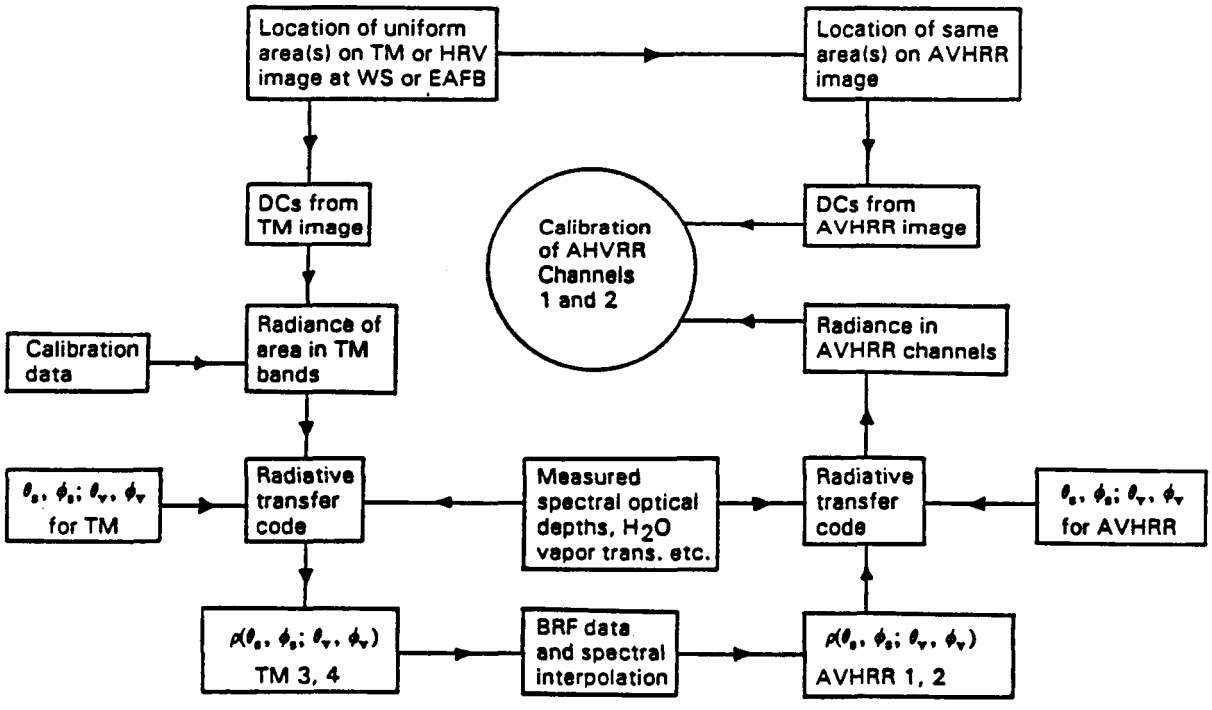

Figure 1. "Method 1" calibration approach: ground and atmospheric measurements and reference to another calibrated satellite sensor.

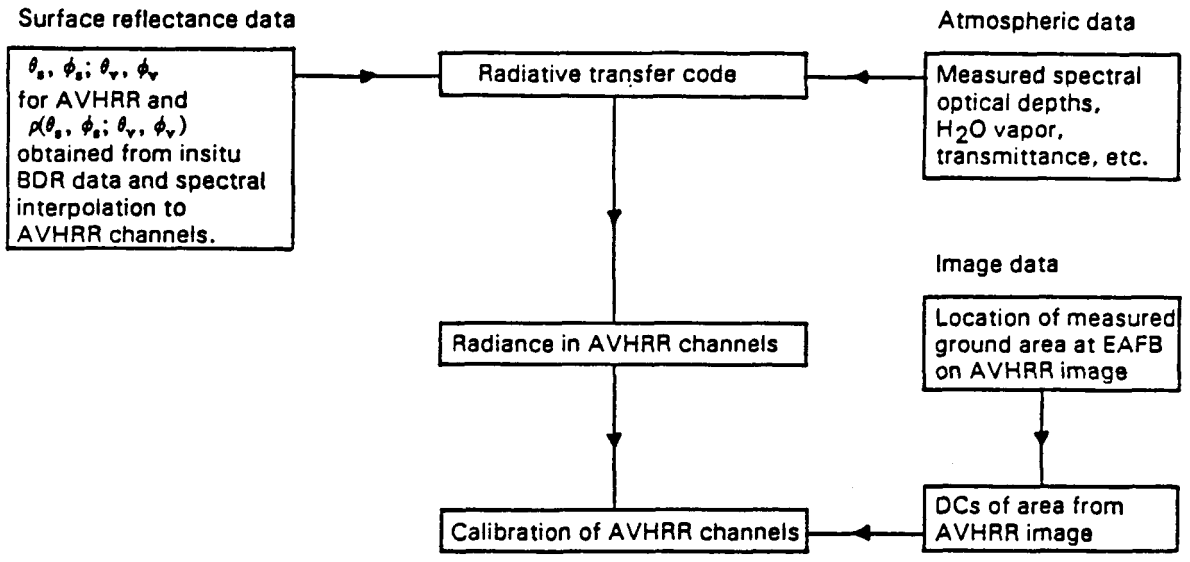

Figure 2. "Method 2" calibration approach: ground and atmospheric measurements without reference to another sensor.

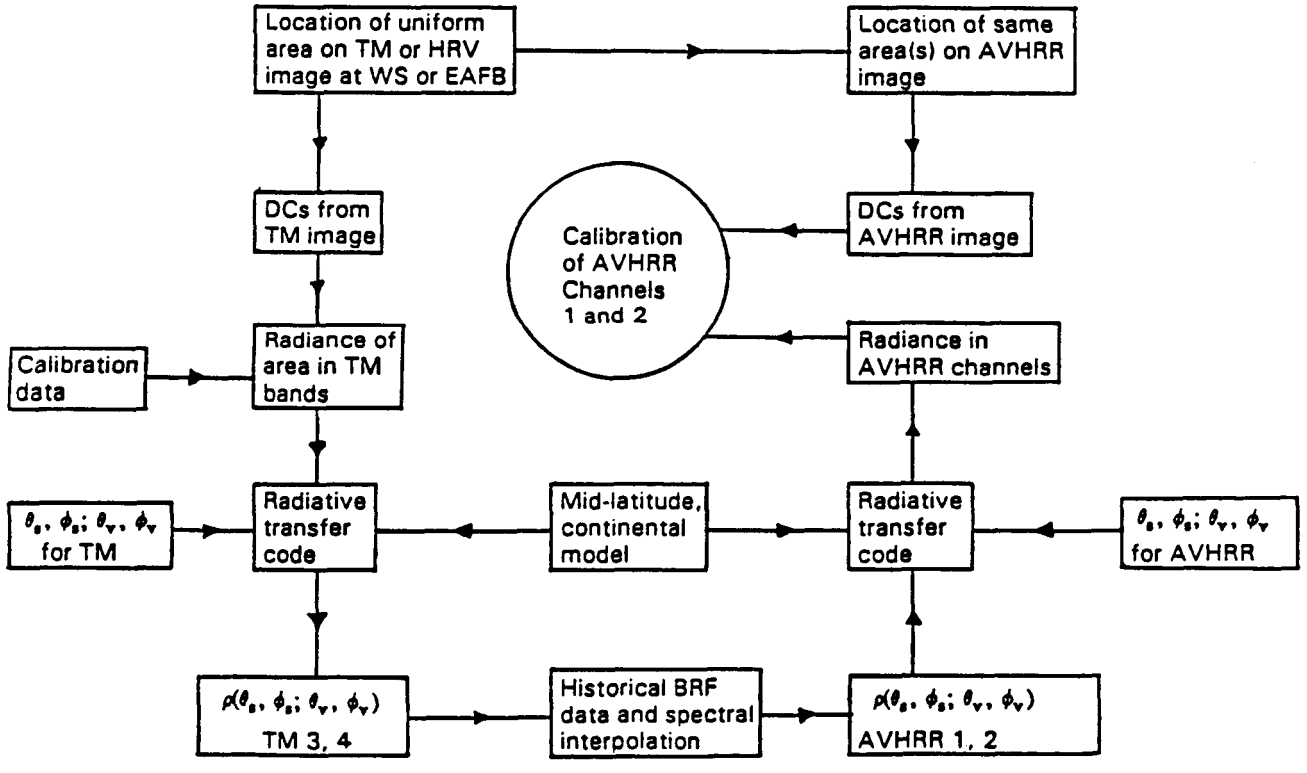

Figure 3. "Method 3" calibration approach: no ground and atmospheric measurements but reference to another satellite sensor.

2. NOAA-9 AND NOAA-10 AVHRR DATA SETS

The methods described in the previous section have been applied to several data sets involving NOAA-9 and NOAA-10 AVHRR imagery. The principal characteristics of these two sensor systems are listed in Table 1. As indicated in the table, prelaunch radiometric calibrations were performed many years prior to launch.

The collection of data sets involving ground-based measurements and/or same-day coverage of a test area by more than one satellite sensor is difficult to accomplish. The logistics and expense of field measurement campaigns as well as ever-present limitations due to weather severely reduce the number of data sets suitable for calibration work. An additional constraint in the case of AVHRR coverage of a given site is the possibility of large off-nadir view angles, which are not used if they exceed 40 to 45 degrees. Nevertheless, several AVHRR data sets have been acquired (Table 2) over the last few years during calibration experiments at White Sands, New Mexico and at the Rogers Dry Lake at Edwards Air Force Base (EAFB) in California. The work at EAFB has been concerned with calibration of airborne sensors and so there is no reference to another satellite sensor for that site (Method 2). At the White Sands Missile Range (WSMR), the main efforts have been directed towards in-flight calibration of the Landsat TM and SPOT HRV sensors.[1,2] Hence, TM or HRV image data are used as the reference in Method 1 and Method 3 analyses. To date, calibration results have been obtained for four NOAA-9 AVHRR cases (August 28, 1985; October 14, 1986; May 4, 1987; May 5, 1987) and for one NOAA-10 AVHRR case (March 27, 1987).

Table 1. Principal characteristics of the NOAA-9 and NOAA-10 AVHRR sensor systems. The indicated spectral bandpass limits are nominal values; the spectral response profiles of the two sensors actually differ somewhat.

	NOAA-9 AVHRR	NOAA-10 AVHRR
Prelaunch Calibration:	approx. February, 1980	approx. March, 1977
Launch Date:	December, 1984	September, 1986
Orbit:	sun-synchronous ascending node (day)	sun-synchronous descending node (day)
Equatorial Crossing:	14:30	07:30
Nadir Resolution:	1.1 km	1.1 km
Scan Angle Range:	± 55.4°	± 55.4°
Spectral Bands (μm):	Ch. 1 (0.58-0.68) Ch. 2 (0.725-1.1) Ch. 3 (3.55-3.93) Ch. 4 (10.3-11.3) Ch. 5 (11.5-12.5)	Ch. 1 (0.58-0.68) Ch. 2 (0.725-1.1) Ch. 3 (3.55-3.93) Ch. 4 (10.3-11.3)
Quantization:	10 bit	10 bit

Table 2. NOAA-9 and NOAA-10 AVHRR data sets. The bracketed number after the date refers to the number of days since launch. WSMR is the White Sands Missile Range in New Mexico and EAFB is Edwards Air Force Base in the Mojave Desert of California.

NOAA-9 AVHRR Data Sets

Date	Site	Reference Sensor	Status
1985.08.28 (260)	WSMR	TM	Completed (Methods 1 and 3)
1986.10.14 (672)	EAFB	--	Completed (Method 2)
1987.05.04 (874)	EAFB	--	Completed (Method 2)
1987.05.05 (875)	EAFB	--	Completed (Method 2)
1988.02.10 (1157)	WSMR	TM, HRV	Planned

NOAA-10 AVHRR Data Sets

Date	Site	Reference Sensor	Status
1987.03.27 (192)	WSMR	TM	Completed (Methods 1 and 3)
1987.03.28 (193)	WSMR	HRV	In Progress
1987.07.17 (305)	WSMR	HRV	In Progress
1987.09.13 (363)	EAFB	--	Planned
1988.02.09 (512)	WSMR	next day TM, HRV	Planned

3. ANALYSIS PROCEDURES

3.1 Method 1 analysis for NOAA-9 AVHRR on August 28, 1985 at WSMR

A geometric registration procedure was used to match the relevant portions of the TM and AVHRR images of White Sands. From the superimposed images, a relatively uniform area of two by two AVHRR pixels was selected in the alkali-flat region. The digital counts for this area and for the corresponding area in the TM imagery were extracted and averaged.

In order to relate the TM radiance values (corresponding to the aforementioned TM digital counts for the AVHRR test area) to ground reflectance factors, a series of atmospheric model computations were carried out using the Herman radiative transfer code.[3] The Rayleigh and aerosol optical depths required by the code were determined from an analysis of Langley plots, in which the log voltages from solar radiometers were plotted against air masses for the satellite overpass day. The result of this step is a set of surface reflectance factors in the TM bands over a much larger area than could be measured using ground-based techniques.

At the NOAA-9 satellite overpass time of 21:27 Coordinated Universal Time (UT), the solar zenith angle was 39.85 degrees, whereas at the Landsat-5 satellite overpass time of 17:08 UT, the solar zenith angle was 35.95 degrees. Moreover, the off-nadir view angle was 23.6 degrees for the AVHRR sensor and about one degree for the TM sensor. Thus, in order to obtain values relevant to the AVHRR conditions, corrections were applied to the TM band 3 and 4 reflectance factors on the basis of bidirectional reflectance (BRF) measurements made for the gypsum surface at a variety of solar zenith angles at White Sands on March 15, 1986. The reflectance factors were further adjusted to the central wavelengths of AVHRR channels 1 and 2.

Atmospheric parameters and surface reflectances for the two AVHRR channels were then input to the Herman radiative transfer code for the return pass through the atmosphere. The result is predicted radiance at the entrance aperture of the AVHRR sensor in each channel. Both for this step and the earlier pass down through the atmosphere for TM, an additional adjustment was applied to correct for gaseous absorption. More specifically, the French "5-S" atmospheric program[4] was run to obtain the total gaseous transmittance for four gases (H_2O, O_3, CO_2, and O_2).

3.2 Method 2 analysis for NOAA-9 AVHRR on three dates at EAFB

Although it makes no reference to another imaging sensor, the Method 2 calibration approach relies on ground-based measurements of atmospheric conditions and surface reflectance made at the site on the day of an overpass with the techniques used at White Sands.[1] Solar radiometer measurements were made next to Rogers Dry Lake at EAFB on October 14, 1986, May 4, 1987, and May 5, 1987. On October 14 and May 5, reflectance factor measurements were made on the dry lakebed over a 320 meter by 80 meter target area related to another experiment. The ground reflectance data were collected using a Barnes MMR in spectral bands similar to the Landsat TM bandpasses. Reflectance factors were computed using a calibrated barium sulfate panel and an average reflectance was computed for the entire target area in each band.

The atmospheric radiative transfer computations require a surface reflectance value as one of the inputs in any given spectral band. However, the measured reflectance factors were acquired with nadir viewing geometry and usually not at AVHRR overpass time (and hence at a different sun angle). Thus, the reflectance factors were corrected to be appropriate for the sun and view angle geometries for the NOAA-9 AVHRR overpasses of EAFB on each of the three dates. These corrections were made with the help of BRF measurements made on the dry lakebed at a variety of solar zenith angles on May 5, 1987, May 6, 1987, and September 14, 1987. A final adjustment was made to the reflectance factors to correspond to the central wavelengths of AVHRR channels 1 and 2. The use of the Herman and "5-S" codes is as described earlier in the Method 1 approach.

Bright and dark features were identified in SPOT HRV and Airborne Visible and Infrared Imaging Spectrometer (AVIRIS) imagery,[5] acquired at other times for the EAFB area, that were also distinguishable in the AVHRR scenes. The features used for this purpose were not likely to have changed places in time and were sufficiently numerous to minimize the effect of systematic geometric distortions. The location of the ground measurement site on the dry lakebed could then be estimated visually in the AVHRR imagery using relative distances and triangulation. Digital image analysis facilities were used for this purpose. The corresponding "best estimate" digital counts were then interpolated from image values in channels 1 and 2.

The surface at Rogers Dry Lake is quite flat for many kilometers in all directions but its reflectance characteristics are reasonably uniform only in a limited area, roughly 1 3/4 kilometers in the predominantly East-West direction. Thus, although that part of the dry lakebed provides a large uniform target for high-resolution sensors, it can accommodate the area of one AVHRR pixel only for off-nadir view angles less than 35 degrees relative to vertical at ground level (the approximate pixel dimensions on the various dates are listed in Table 3). Because this site is not easy to pin-point in the AVHRR imagery, digital counts were also obtained by interpolation for locations plus or minus half a pixel away in the direction of the strongest radiance gradient.

Table 3. Sun and view angle geometries for the NOAA-9 and NOAA-10 AVHRR overpasses. The nadir view angles are relative to vertical at ground level and view azimuth angles are in the satellite direction from the ground location.

Date	Overpass Time (U.T.)	Solar Zenith (Degrees)	Solar Azimuth (Degrees)	Solar Distance (A.U.)	Off-Nadir View (Degrees)	View Azimuth (Degrees)	Approximate Pixel Dimensions (km)
1985.08.28	21:27:00	39.9	242.1	1.0098	23.6	259	1.4 x 1.3
1986.10.14	21:46:55	53.0	221.6	0.9972	44.5	259	2.2 x 1.6
1987.05.04	22:29:54	40.7	252.8	1.0087	15.3	79	1.3 x 1.2
1987.05.05	22:19:03	38.5	250.8	1.0087	31.3	79	1.6 x 1.3
1987.03.27	15:15:45	62.7	107.0	0.9979	21.5	281	1.3 x 1.2

3.3 Method 3 analysis for NOAA-9 AVHRR on August 28, 1985 at WSMR

Although the data flow for this method schematically resembles that of Method 1, it differs considerably in nature in that no ground-based measurements of atmospheric conditions and surface reflectance are required. The actual atmosphere is approximated by a standard set of atmospheric conditions and the "5-S" atmospheric model is invoked as a simpler and faster code to use. Historical BRF data are used to adjust TM reflectance factors to the illumination and viewing geometries pertinent to the AVHRR overpass. In other respects, the analysis procedure is identical to Method 1.

It is also of interest to test the sensitivity of Method 3 to the assumed atmospheric characteristics. In particular, the "5-S" code allows the user to easily modify input specifications for visibility, aerosol model, and atmospheric profile.[4,6] The different cases examined are listed in Table 4. The nominal case for the White Sands area is 100 kilometer visibility, continental aerosols, and a mid-latitude summer profile.

Table 4. Sensitivity analysis selections for input to the "5-S" code used in Method 3 calibration analyses.

Visibility (km)	Aerosol Model	Atmospheric Model
200	Continental	Mid-Latitude Summer
100	Continental	Mid-Latitude Summer
50	Continental	Mid-Latitude Summer
23	Continental	Mid-Latitude Summer
200	Maritime	Tropical
100	Maritime	Tropical
50	Maritime	Tropical
23	Maritime	Tropical
200	Continental	Sub-Arctic Winter
100	Continental	Sub-Arctic Winter
50	Continental	Sub-Arctic Winter
23	Continental	Sub-Arctic Winter

3.4 Method 1 and Method 3 analyses for NOAA-10 AVHRR on March 27, 1987 at WSMR

Compared to the Method 1 and Method 3 analyses for NOAA-9 AVHRR, the only differences in the case of the NOAA-10 AVHRR concern image data manipulation. Unlike the situation with NOAA-9, the NOAA-10 AVHRR and the Landsat TM sensors acquire images from similar orbital configurations (descending orbit). Thus, no significant rotation was necessary to superimpose the two image data sets and the main factor to be dealt with was the different off-nadir viewing angles involved.

The other difference is not inherent to the NOAA-10 AVHRR sensor but rather concerns the adoption of a different procedure for selecting common areas in the TM and AVHRR scenes. More specifically, the TM scene was examined on a digital image display for relatively uniform patches greater than one AVHRR pixel in extent. Ten such locations were identified, seven in the alkali-flat region for use in the actual analysis and three in the dunes area for comparison. Block averages of 45 pixels by 41 lines (corresponding to the size of one AVHRR pixel) were obtained in TM bands 3 and band 4 image data centered in each of the ten areas. The central locations were then identified in the registered AVHRR imagery and corresponding digital counts were obtained from AVHRR channels 1 and 2. Because each of the uniform image patches were well over one AVHRR pixel in extent and only one AVHRR sample was taken from each such area, problems due to mis-registration should have been minimized. Figure 4 shows that there is some merit to this approach. It plots digital counts from AVHRR channel 1 against TM band 3 and AVHRR channel 2 against TM band 4 after geometric registration, with linear regressions yielding coefficients of determination of 0.993 and 0.984, respectively. By means of such graphs, outliers could be removed from further analysis. However, all seven points were kept for the purposes of this exploratory work.

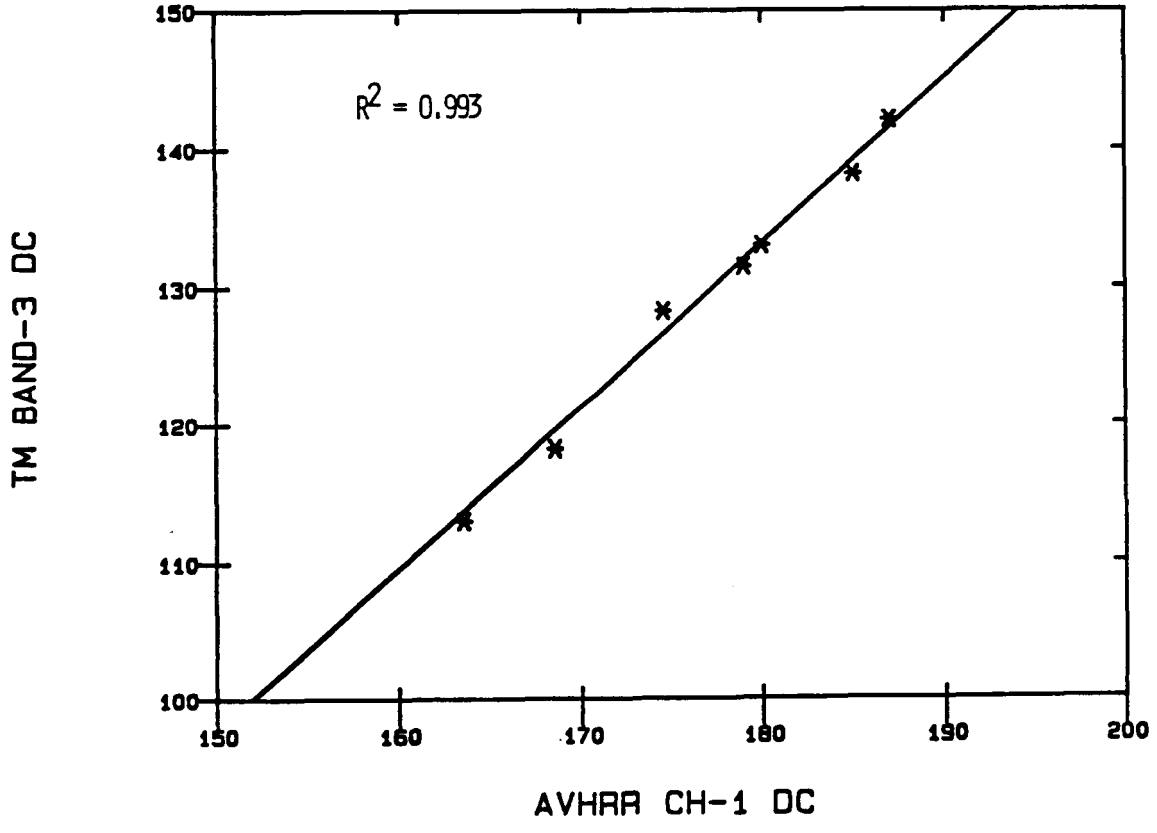

Figure 4(a). Comparison of digital counts from AVHRR channel 1 and TM band 3 on March 27, 1987 for seven locations in the alkali-flats region at White Sands after geometric registration. The straight line is a linear regression fit.

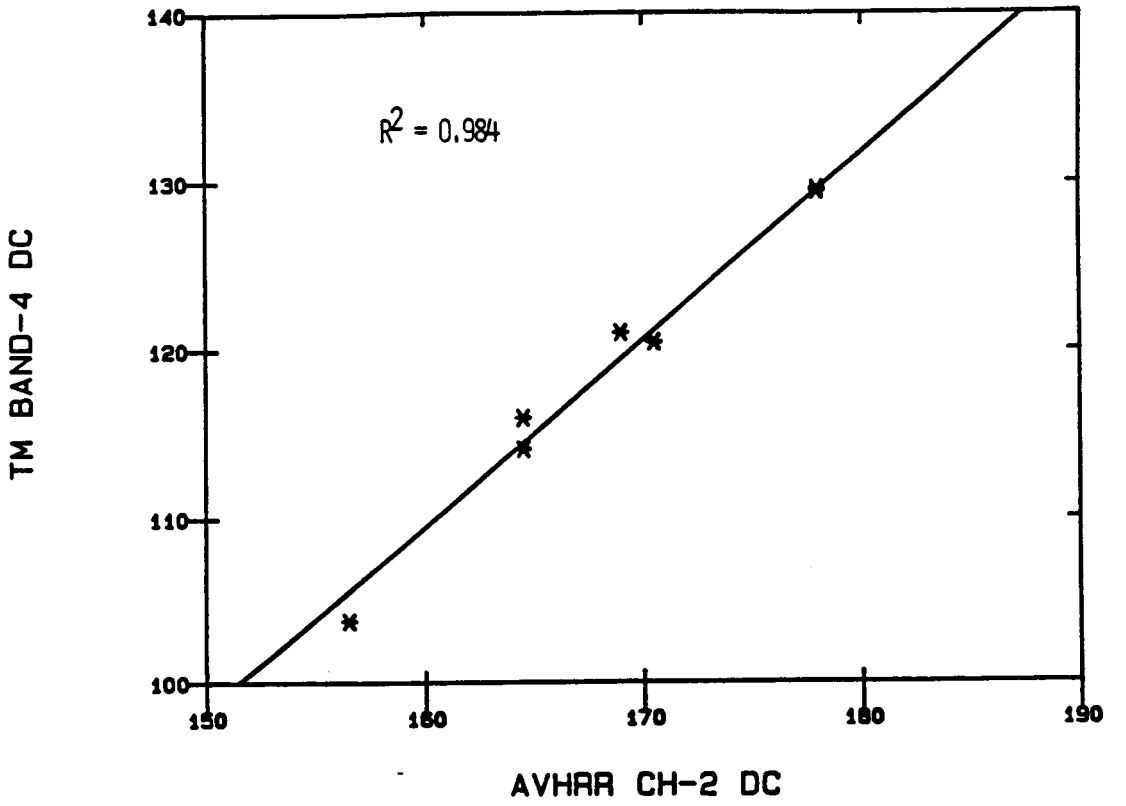

Figure 4(b). Comparison of digital counts from AVHRR channel 2 and TM band 4 on March 27, 1987 for seven locations in the alkali-flats region at White Sands after geometric registration. Two points fall in the same place (the brightest location) and so only six points are distinguishable in the plot. The straight line is a linear regression fit.

4. RESULTS

4.1 NOAA-9 AVHRR Calibration

Absolute calibration coefficients for the reflective channels of the NOAA-9 AVHRR are listed in Table 5 and portrayed as a function of time in Figures 5(a) and 5(b). It is evident that the sensor's responsivity has degraded significantly with time, with the greater change occurring in channel 2. That the gain coefficients in October 1986 should be somewhat higher than in May 1987 is largely due to the difficulty in making a precise BRF correction for the earlier date when the off-nadir view angle was nearly 45 degrees, but also partly due to the problem of having a

Table 5. NOAA-9 AVHRR radiometric calibration results. For Method 2 at EAFB, results are given in parentheses for locations plus or minus half a pixel away in the scan direction. Gain coefficients are in units of $Wm^{-2}sr^{-1}\mu m^{-1}count^{-1}$.

Date	Method	Channel 1 Gain		Channel 2 Gain	
Prelaunch		0.5243		0.3286	
1985.08.28	1	0.552		0.390	
1986.10.14	2	0.703	(0.654, 0.732)	0.470	(0.437, 0.491)
1987.05.04	2	0.674	(0.649, 0.697)	0.447	(0.430, 0.462)
1987.05.05	2	0.666	(0.631, 0.705)	0.436	(0.413, 0.463)

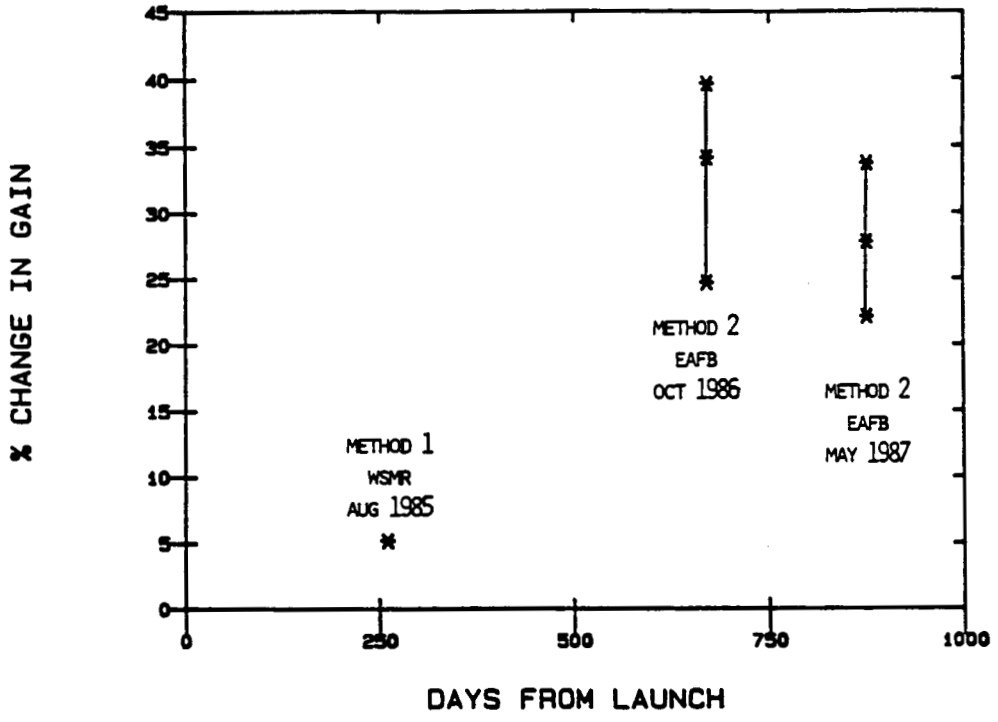

Figure 5(a). NOAA-9 AVHRR channel 1 calibration results expressed as percent change in gain as a function of time. In Method 2 cases at EAFB, results for locations plus or minus half a pixel away in the scan direction give rise to the error bars. The May 1987 results are averages from May 4 and May 5.

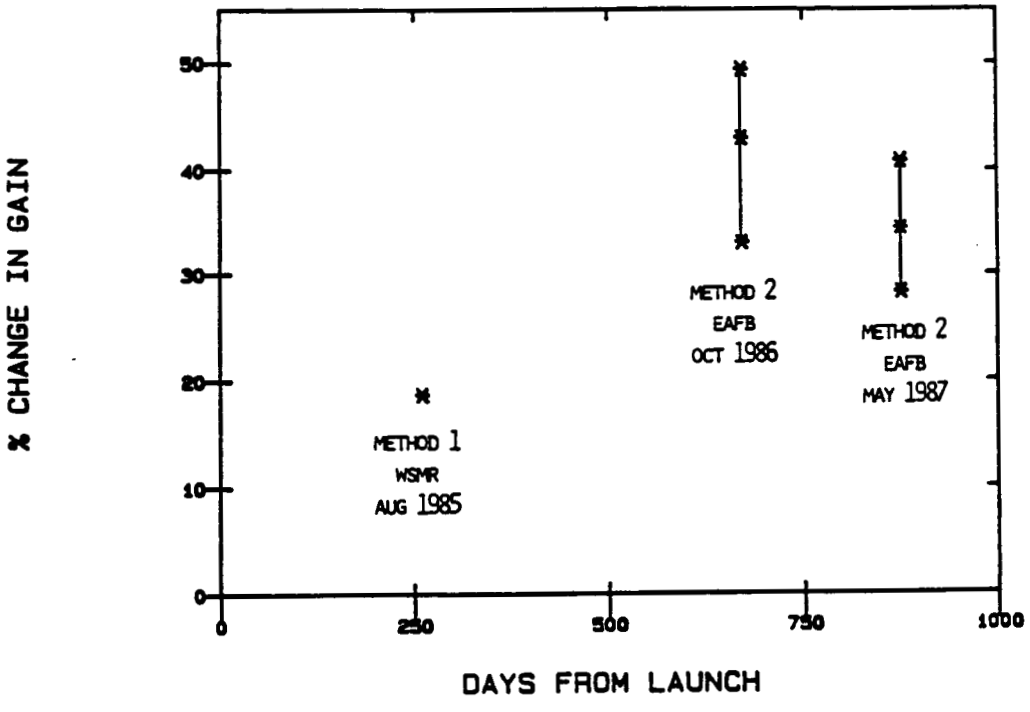

Figure 5(b). As for Figure 5(a), except for NOAA-9 AVHRR channel 2.

2.2 kilometer pixel dimension in the scan line direction, which exceeds the size of the uniform reflectance patch at EAFB. The results for May 4 and May 5, 1987 are reasonably consistent. Although the same surface reflectance measurements were used for both days since no reflectance measurements were made on May 4th, different atmospheric parameters were used and the off-nadir view angles differed considerably (Table 3). No detailed error analysis has been carried out for the Method 1 approach, but a rough estimate indicates an uncertainty on the order of 5 percent.

Method 3 and Method 1 calibration results on August 28, 1985 are compared in Table 6. Lacking any knowledge of atmospheric conditions at White Sands, the standard conditions would be assumed to be a mid-latitude summer profile with continental aerosols and a visibility of 100 km. The difference between the two methods in that case would be 1.6% in channel 1 and 2.7% in channel 2. There appears to be very little sensitivity to the assumed visibility and a slight sensitivity to a change to a moister atmosphere (tropical) with maritime aerosols. The greatest effect in this regard occurred in channel 2 with a change to a drier atmosphere (sub-arctic winter). Notable differences between the two methods also arise if no corrections are made for sun angle, view angle, and wavelength differences between the TM and AVHRR conditions.

Table 6: Method 3 calibration results for NOAA-9 for August 28, 1985. M.L.S. = Mid-Latitude Summer; S.A.W. = Sub-Arctic Winter; Trop. = Tropical; Cont. = Continental; Marit. = Maritime. "Matched" refers to 5S runs using measured aerosol and Rayleigh optical depth values. Gain coefficients are in units of $Wm^{-1}sr^{-1}\mu m^{-1}count^{-1}$.

Visibility (km)	Atmospheric Profile	Aerosol Model	Channel 1 Gain	Difference from Method 1	Channel 2 Gain	Difference from Method 1
200	M.L.S.	Cont.	0.540	-1.5%	0.373	-2.7%
100	M.L.S.	Cont.	0.540	-1.6%	0.373	-2.7%
50	M.L.S.	Cont.	0.539	-1.7%	0.373	-2.8%
23	M.L.S.	Cont.	0.539	-1.9%	0.372	-2.9%
200	Trop.	Marit.	0.544	-0.9%	0.370	-3.5%
100	Trop.	Marit.	0.544	-0.9%	0.370	-3.4%
50	Trop.	Marit.	0.545	-0.7%	0.371	-3.2%
23	Trop.	Marit.	0.548	-0.2%	0.372	-2.9%
200	S.A.W.	Cont.	0.535	-2.4%	0.389	+1.5%
100	S.A.W.	Cont.	0.535	-2.5%	0.389	+1.5%
50	S.A.W.	Cont.	0.534	-2.6%	0.389	+1.4%
23	S.A.W.	Cont.	0.533	-2.8%	0.388	+1.2%
With no BRF and no λ adjustment						
200	M.L.S.	Cont.	0.535	-2.6%	0.362	-5.6%
50	M.L.S.	Cont.	0.534	-2.7%	0.362	-5.7%
"Matched"	M.L.S.	Cont.	0.541	-1.3%	0.382	-0.2%
	Method 1 results:		0.549		0.383	
	Prelaunch values:		0.5243		0.3286	

4.2 NOAA-10 AVHRR Calibration

Absolute calibration coefficients based on Method 1 for the reflective channels of the NOAA-10 AVHRR on March 27, 1987 are given in Table 7. Compared to prelaunch values, the mean gain coefficients for the seven alkali-flats locations represent degradations of 21% and 35% in the responsivities of channels 1 and 2, respectively. Results for the dunes differ considerably from those for the alkali-flats, probably because the BRF corrections based on data acquired at Chuck Site are not applicable to the dunes area. Conversely, the consistency between results for the various alkali-flats locations indicates that the

Table 7. NOAA-10 AVHRR radiometric calibration results based on Method 1 for March 27, 1987 at White Sands. The first seven locations listed are in the alkali-flats region. Gain coefficients are in units of $Wm^{-2}sr^{-1}\mu m^{-1}count^{-1}$.

Location	Channel 1 Gain	Channel 2 Gain
#1	0.603	0.445
#2	0.626	0.467
#3	0.623	0.472
#4	0.621	0.464
#5	0.633	0.474
#6	0.606	0.460
#7	0.629	0.473
Mean	0.621	0.465
Std. Dev.	0.019	0.016
Prelaunch	0.5115	0.3454
#1 (dunes)	0.686	0.509
#2 (dunes)	0.675	0.504
#3 (dunes)	0.624	0.476

BRF corrections can be extended widely in that region of White Sands. Method 3 and Method 1 calibration results on March 27, 1987 are compared in Table 8. As for the case discussed in the previous section, results from the two methods are generally within a few percent of each other. The greatest difference occurs in channels 2 if the atmosphere is assumed to be a sub-artic winter model.

5. DISCUSSION

A significant degradation in NOAA-9 AVHRR responsivity has occurred since the prelaunch calibration and with time since launch. As of May 1987, the change has been on the order of 25 to 30 percent in channel 1 and approximately 35 percent in channel 2. The analysis of more recent data sets is needed to update and further characterize the degradation. In this regard, a data set involving TM, HRV, and AVHRR imagery is currently being assembled after a successful field trip to White Sands on February 8-10, 1988.

Table 8: Method 3 calibration results for NOAA-10 for March 27, 1987. M.L.S. = Mid-Latitude Summer; S.A.W. = Sub-Arctic Winter; Trop. = Tropical; Cont. = Continental; Marit. = Maritime. Gain coefficients are in units of $Wm^{-2}sr^{-1}\mu m^{-1}count^{-1}$.

Visibility (km)	Atmospheric Profile	Aerosol Model	Channel 1 Gain	Difference from Method 1	Channel 2 Gain	Difference from Method 1
200	M.L.S	Cont.	0.631	+1.6%	0.481	+3.4%
100	M.L.S.	Cont.	0.628	+1.1%	0.479	+3.0%
50	M.L.S.	Cont.	0.625	+0.6%	0.475	+2.2%
23	M.L.S.	Cont.	0.622	+0.2%	0.467	+0.4%
200	Trop.	Marit.	0.635	+2.3%	0.475	+2.2%
100	Trop.	Marit.	0.634	+2.1%	0.473	+1.7%
50	Trop.	Marit.	0.634	+2.1%	0.471	+1.3%
23	Trop.	Marit.	0.634	+2.1%	0.470	+1.1%
200	S.A.W.	Cont.	0.618	-0.5%	0.506	+8.8%
100	S.A.W.	Cont.	0.616	-0.8%	0.504	+8.4%
50	S.A.W.	Cont.	0.613	-1.3%	0.500	+7.5%
23	S.A.W.	Cont.	0.609	-1.9%	0.492	+5.8%
With no BRF and no λ adjustment:						
200	M.L.S.	Cont.	0.618	-0.5%	0.461	-0.9%
50	M.L.S.	Cont.	0.613	-1.3%	0.455	-2.2%
	Method 1 results:		0.621		0.465	
	Prelaunch values:		0.5115		0.3454	

With only one data set analyzed so far, the analysis of additional data sets is needed to assess any changes in NOAA-10 AVHRR calibration. As of March 1987, the degradation from the prelaunch calibration is on the order of 21 percent in channel 1 and 35 percent in channel 2.

There are some limitations to the use of Method 2 with the Rogers Dry Lake site at Edwards Air Force Base. The uniform area is limited to one AVHRR pixel (for nadir view angles less than 35 degrees relative to vertical at ground level) and is surrounded by terrain of much brighter and much darker reflectance on either side. In addition, unlike the gypsum at White Sands, the surface is not very lambertian so that accurate BRF corrections are important. (It should also be noted that the radiative transfer codes used assume lambertian reflectance.) Method 2 using the Rogers Dry Lake site is not likely to be able to track gain changes less than about 10 percent.

In both Methods 1 and 3, corrections for sun angle, view angle, and spectral differences between the higher resolution data and the AVHRR data are important, as is a good calibration of the high resolution sensor. For the data sets analyzed to date, the alkali-flats area at White Sands has proven to be quite suitable for the Method 1 and Method 3 approaches.

As far as Method 3 is concerned, results are generally within 1 to 3 percent of Method 1 for the conditions usually expected at White Sands. The method is not very sensitive to assumed visibility and hence aerosol optical depth, but it does show some sensitivity to the assumed atmospheric profile and hence water vapor, especially in channel 2. Nevertheless, the results for Method 3, which requires no field measurements and makes use of a simplified atmospheric model, are very promising. Because the results from this approach compare favorably with the more detailed methods and are not overly sensitive to assumed atmospheric conditions, the implication is that a reasonable calibration of satellite sensors may be possible by transfer, without the necessity of making ground-based measurements. In this way, it would be relatively straightforward to monitor occasionally (and retrospectively as well) the status of AVHRR sensor radiometric responses.

6. ACKNOWLEDGEMENTS

We wish to thank G. Smith and B. Markham for their help in providing digital imagery, as well as R. Frouin, C. Whitlock, and G. Vane for useful discussions. We also wish to thank B. M. Herman for the use of his radiative transfer code and J. A. Reagan for the use of his solar radiometer. The work at the University of Arizona was supported by NASA grant NAG5-859.

7. REFERENCES

1. Slater, P. N., S. F. Biggar, R. G. Holm, R. D. Jackson, Y. Mao, M. S. Moran, J. M. Palmer, and B. Yuan, "Reflectance- and radiance-based methods for the in-flight absolute calibration of multispectral sensors", Remote Sensing of Environment, 22:11-37 (1987).

2. Begni, G., M. C. Dinguirard, R. D. Jackson, and P. N. Slater, "Absolute calibration of the SPOT-1 HRV cameras", Proc. SPIE, Vol. 660, Earth Remote Sensing Using the Landsat Thematic Mapper and SPOT Sensor Systems, pp. 66-76 (1986).

3. Herman, B. M. and S. R. Browning, "The effect of aerosols on the earth-atmosphere albedo, J. Atmos. Sci., 32:158-165 (1975).

4. Tanré, D., C. Deroo, P. Duhaut, M. Herman, J. J. Morcrette, J. Perbos, and P. Y. Deschamps, "Effets atmosphériques en télédétection-logiciel de simulation du signal satellitaire dans le spectre solaire", Proc. Third Int. Colloq. on Spectral Signatures of Objects in Remote Sensing, ESA SP-247, pp. 315-319 (1985).

5. Vane, G., Jet Propulsion Laboratory, California, communication to the authors (1987).

6. McClatchey, R. A., R. W. Fenn, J. E. A. Selby, F. E. Volz, and J. S. Garing, "Optical properties of the atmosphere", Report AFCRL-71-0279, Environmental Research Papers, No. 354, AFCRL, Hanscom Field, Bedford, MA (1971).

APPENDIX 2.

Laboratory calibration of field reflectance panels

S. F. Biggar[1], J. Labed[1,3], R. P. Santer[1,4], P. N. Slater[1], R. D. Jackson[2], and M. S. Moran[2].

[1] Optical Sciences Center, University of Arizona, Tucson, Arizona 85721.
[2] U.S. Department of Agriculture, U.S. Water Conservation Laboratory, Phoenix, Arizona 85040.
[3] On leave from the l'Université Louis Pasteur, F-67000 Strasbourg, Cedex France
[4] On leave from the Laboratoire d'Optique Atmosphérique, Université des Sciences et Techniques de Lille, 59655 Villeneuve d'Ascq Cédex, France.

ABSTRACT

A method used for calibrating field reflectance panels in the visible and shortwave infrared wavelength range is described. The directional reflectance factor of painted barium sulfate ($BaSO_4$) panels is determined. The reference for this method is the hemispherical reflectance of pressed polytetrafluoroethylene (halon) powder prepared according to National Bureau of Standards (NBS) directions. The panels and a radiometer are mounted on rotation stages to measure the reflectance factor at different incidence and view angles. The sensor can be any laboratory or field filter radiometer small enough to mount on the apparatus.

The method is used to measure the reflectance factors of halon and $BaSO_4$ panels between 0.45 and 0.85 micrometers. These reflectance factors are compared to those measured by a field apparatus. The results agree to within 0.013 in reflectance at incidence angles between 15 and 75 degrees.

1. INTRODUCTION

It is necessary to know the reflectance factor of target materials for various remote sensing applications. In many cases the reflectance is determined by reference to a calibrated field reflectance standard. The standard is usually either a painted $BaSO_4$ panel or a pressed halon panel. In order to use these panels to accurately determine the reflectance of the target, the standard panels must be calibrated because they are not perfectly lambertian reflectors. Because these panels are used with a nadir viewing angle under varying conditions of illumination (the solar zenith angle changes during the period of observations), the directional reflectance factor of the panels must be determined.

Ideally, a reflectance panel should be calibrated using the same source and sensor that will be used for field measurements. Indeed, a field calibration method was recently reported[1]. However, the field method requires clear skies and constant atmospheric conditions during the measurement period. The scheduling of calibrations is thereby controlled by the weather, and not by the needs of the investigator. Calibrations made in a laboratory setting are not subject to these constraints and, in most cases, the illumination and measurement geometry can be held to considerably higher accuracies. This report describes a laboratory facility and methodology for calibrating reference reflectance standards.

A valuable extension to the use of the reflectance panel calibration apparatus is the calibration of portable radiometers. If a calibrated reflectance panel is mounted on the apparatus at an accurately known distance from a standard source of spectral irradiance, the panel provides a surface of known spectral radiance. Voltage outputs from a portable radiometer can then be associated with the spectral radiances within each band of the radiometer when the integrated relative spectral response across each band has been independently determined.

2. CALIBRATION FACILITY AND METHODOLOGY

2.1 Equipment and fixtures

Three fixtures comprise the laboratory set up. The first is an L-shaped arm which supports the radiometer. The arm has an interchangeable mount to accommodate different radiometers. It holds the center of the radiometer's entrance pupil 50 cm away from the center of the panel and it aligns the radiometer's optical axis in the plane containing incident illumination beam and the panel normal.

The second fixture is the panel holder. It keeps the panel's front surface coincident with the vertical axis of rotation of the stage. The panel can be as large as 24 inches on a side. The entire set up is aligned by securing a mirror to the empty panel holder and placing a laser behind the source so that its beam coincides with the optical axis of the illumination source.

The lamp that provides illumination and its holder are the third fixture, which is mounted to a table. The holder allows three orthogonal translations, two orthogonal tilts and a rotation of the source. A large vertical screen with a circular aperture of 3-cm diameter restricts illumination to the center of the panel. Figure 1 is a block diagram (not to scale) of the equipment layout. Both the arm and the panel holder are fastened to a rotary stage; the stages are stacked with the base of the top stage fastened to the rotating platform of the bottom stage. The base of the bottom stage is rigidly fastened to the same table as the lamp holder. All the elements are made of aluminum. They are anodized or painted flat black to reduce stray reflections.

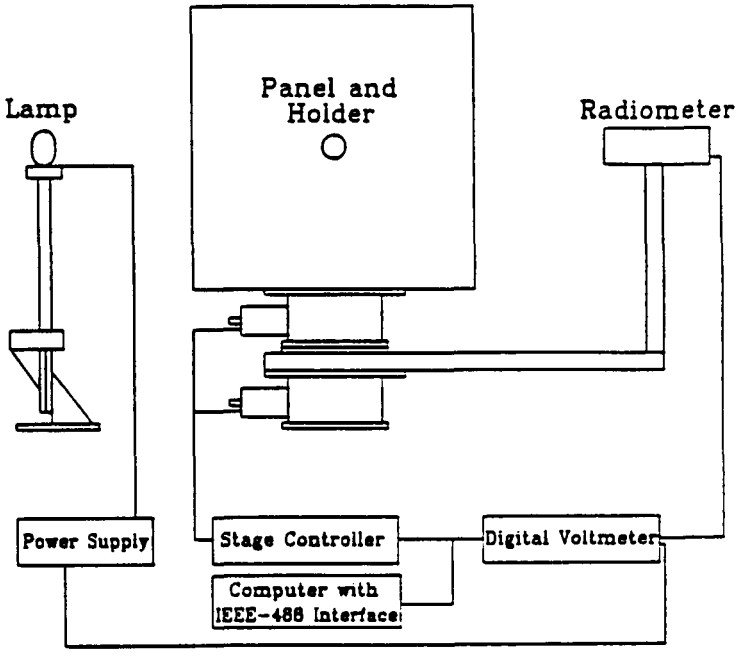

Figure 1. Reflectance measurement layout.

2.2 Motion control and data acquisition

Angular scanning in both incidence and viewing angles is achieved by two rotary positioning stages featuring resolution of 6 arc sec and absolute accuracy on the order of 0.1 arc min. Motor and stage control is provided by a microprocessor-based controller. The stages, motors and controller are made by Aerotech*. We estimate the accuracy of the angular alignment of the system to be better than ± 0.1 degree.

The apparatus does not use a chopper, because certain field radiometers do not have provisions for chopping. Therefore, a high accuracy digital voltmeter is used to measure the radiometer output. The voltmeter used is a Hewlett Packard Model HP3457A because it offers good AC line rejection, measurement speed, resolution, accuracy, and remote programming via an external computer. The data acquisition and motion control is commanded by a MS DOS personal computer configured with an IEEE-488 interface. Control and analysis software is written in C.

* Reference to manufacturers does not imply endorsement by the organizations to which the authors are affiliated.

2.3. Radiometer and source

Two radiometers were used in the laboratory. The first was a locally manufactured instrument provided with six manually interchangeable spectral filters on the front. Their band center wavelengths are 0.45, 0.50, 0.55, 0.65, 0.75 and 0.85 μm. This radiometer has a nominal 1-degree full FOV and a silicon detector.

The second radiometer was a four-band, silicon detector radiometer with internal filters which simulate the first four Thematic Mapper (TM) bands. It is made by Exotech. It is used for field ground-reflectance measurements and radiance measurements made from aircraft. The FOV is either 1 or 15 degrees. The radiometer holder has been designed such that any one of the four detectors is aligned with the equipment axis.

The radiometer fixture can also hold a Barnes Modular Multispectral Radiometer (MMR). Although the MMR has not been used for panel calibrations, we have calibrated one using this equipment[2].

The sources are FEL or DXW type, 1-kW quartz halogen lamps, powered by two Hewlett Packard 6274B DC power supplies connected in an autoseries constant current configuration. The lamp current is monitored by measuring the voltage across a precision 0.01 ohm shunt from Leeds and Northrup.

2.4 Noise and integration time.

The HP3457A has programmable integration time. To ensure a good compromise between measurement time and noise rejection, three sets of 100 measurements, at integration times of 1, 10 and 100 power line cycles, were made. The 10 power line cycles integration time gave the lowest standard deviation, probably due to an interaction between integration time and variation in lamp output over the total measurement period. This is illustrated in Table 1.

Table 1: Integration time versus noise

Power line cycles	1	10	100
Output (volts)	3.243	3.248	3.247
σ (volts)	0.0028	0.0012	0.0013
elapsed time (sec)	19	55	416

In order to determine how sensitive the irradiance was to variation in the lamp current, the flux reflected by the halon with normal illumination was measured 10 degrees from the normal, while the current through the lamp was varied from 7.5 to 8.45 amps. If the current was set to 8.0 amps, a variation of 0.001 amps resulted in a change of 0.0125% in the radiometer voltage. Maintaining this low error in current appears reasonable unless the AC line supply varies significantly.

2.5 Halon reference

For each set of measurements, a freshly pressed halon panel 10.8 cm in diameter and 1 cm thick was made in the laboratory following the procedures outlined by Weidner et al[3]. It was smaller than the $BaSO_4$ panel and because of the non-ideal out-of-field rejection characteristics of the radiometer, attention had to be paid to the area surrounding the halon. For this reason a hole the size of the halon panel was cut in the center of a damaged $BaSO_4$ panel, and the halon was placed within the surrounding $BaSO_4$ panel whenever the halon panel was measured as the standard.

3. DERIVATION OF DIRECTIONAL REFLECTANCE FACTOR

The hemispherical reflectance factor of the halon, R_R^h, may be calculated[4] for normally incident light from the angular variations of the reflectance factor $R_R(0^o; \theta)$:

$$R_R^h = \frac{\int_0^{\pi/2} R_R\,(0^o; \theta)\cos\theta \sin\theta\, 2\pi\, d\theta}{\int_0^{\pi/2} \cos\theta \sin\theta\, 2\pi\, d\theta}. \tag{1}$$

Dividing by $R_R\,(0^o; 45^o)$, Equation (1) can be written as:

$$\frac{R_R^h}{R_R\,(0^o; 45^o)} = 2\int_0^{\pi/2} \frac{R_R\,(0^o; \theta)}{R_R\,(0^o; 45^o)} \sin\theta \cos\theta\, d\theta\,. \tag{2}$$

In terms of measurable quantities, Equation (2) can be rewritten as:

$$\frac{R_R^h}{R_R\,(0^o; 45^o)} = 2\int_0^{\pi/2} B(0^o; \theta) \sin\theta \cos\theta\, d\theta \tag{3}$$

where

$$B(0^o; \theta) = \frac{\Phi(0^o; \theta)/\cos\theta}{\Phi(0^o; 45^o)/\cos\,(45^o)} \tag{4}$$

with Φ as the reflected flux from the sample.

$B(0^o; \theta)$ can be approximated by a fifth order polynomial in θ : $B(0^o; \theta) = \sum_{i=0}^{5} b_i\, \theta^{\,i}$. (5)

Inserting Equation (5) into Equation (3), the result becomes a summation:

$$\frac{R_R^h}{R_R\,(0^o; 45^o)} = 2\sum_{i=0}^{5} b_i\, I_i \tag{6}$$

where

$$I_i = \int_0^{\pi/2} \theta^{\,i} \sin\theta \cos\theta\, d\theta. \tag{7}$$

With the measurement results fitted to a fifth order polynomial, Equation 6 was solved for $R_R(0^o; 45^o)$. Then $R_R(0^o; \theta)$ was calculated from the angular measurements as described in the following sections.

4. EXPERIMENTAL PROCEDURE AND RESULTS

4.1 Procedure

Before a measurement was made, the screen aperture in front of the source and the radiometer entrance aperture were covered and a reading was taken to determine the input offset voltage of the amplifier. This dark value was as high as 0.4% of the smallest signal (at 450 nm).

The halon panel was measured at six wavelengths (450, 500, 550, 650, 750, 850 nm) and angles between 10 and 80 degrees at 5 degree intervals. One hundred readings were taken at each position and averaged. The dark value was subtracted from the average. The voltages were converted to $B(0^o; \theta)$ using equation (4). The $B(0^o; \theta)$ were fitted by the least squares method. An individual datum did not deviate from the fitted curve by more than 0.001 and was normally within ± 0.0002. Figure 2 shows a typical fit of data for halon at λ = 450 nm. R_R $(0^o; 45^o)$ was calculated from the measurements and the NBS published value[3,5] of R_R^h according to Equation 6. R_R $(0^o; \theta)$ was then calculated from a set of voltages at different angles. Reflectance factors for all six wavelengths decreased with increasing incidence angle and were nearly independent of wavelength, the largest decrease being at λ = 850 nm for angles greater than 75 degrees. The data demonstrate the non-lambertian properties of the pressed halon.

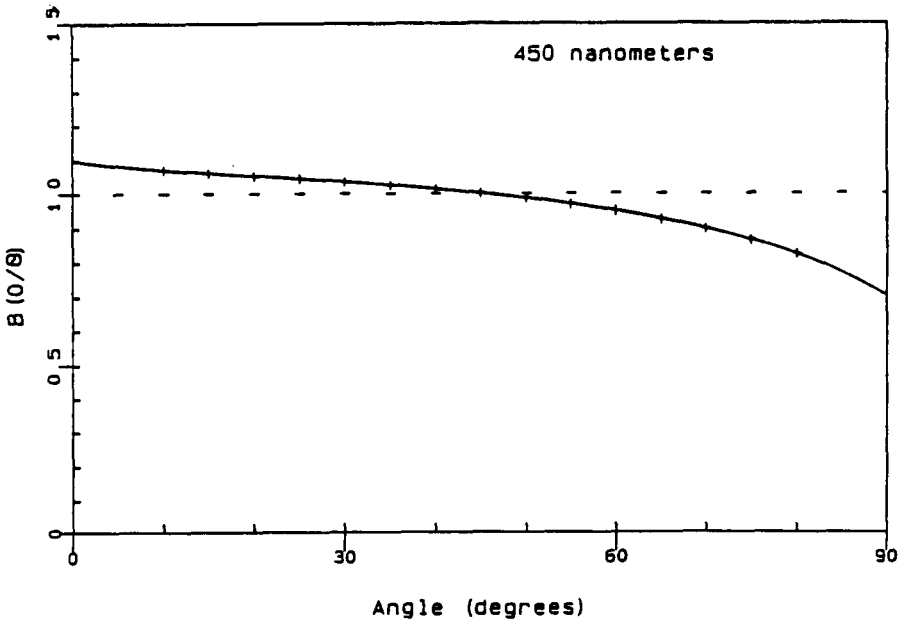

Figure 2. Fitted B coefficient for halon.

The measurements for a single halon panel were made five times under the same conditions. The results were very consistent. The mean value of R_R $(0^o; \theta)$ was calculated for each incident angle and the difference from the mean was computed. For λ = 450 nm, the maximum departure was less than ± 0.002 but was typically within ± 0.0001. At λ = 850 nm, the range of differences from the mean was lower than ± 0.00035.

4.2 $BaSO_4$ panel calibrations

The data for the $BaSO_4$ panel were acquired in the same way as for the halon panel. The bidirectional reflectance factor (BRF) at a particular angle, θ, was found by ratioing the flux (voltage) from the $BaSO_4$ panel with that from the halon panel and multiplying by the halon directional reflectance.

Three reference panels, numbered #1, #2 and #3 for identification purposes, were calibrated. They were constructed at the Optical Sciences Center Infrared Laboratory. The procedures in painting the three $BaSO_4$ panels were similar to the procedure outlined in reference 6.

Values of $R(0^o; \theta)$ for panel #1 for the six wavelengths and for $10 \leq \theta \leq 80$ degrees are shown in Figure 3. BRFs decrease with increasing incidence angle for all wavelengths. The shape of the curves is similar. BRFs for the other two panels, not given here, differ distinctly from #1, whereas they are substantially similar to each other. Panels #2 and #3 are less reflective at small incidence angles and their reflectance factors decrease more slowly with incidence angle.

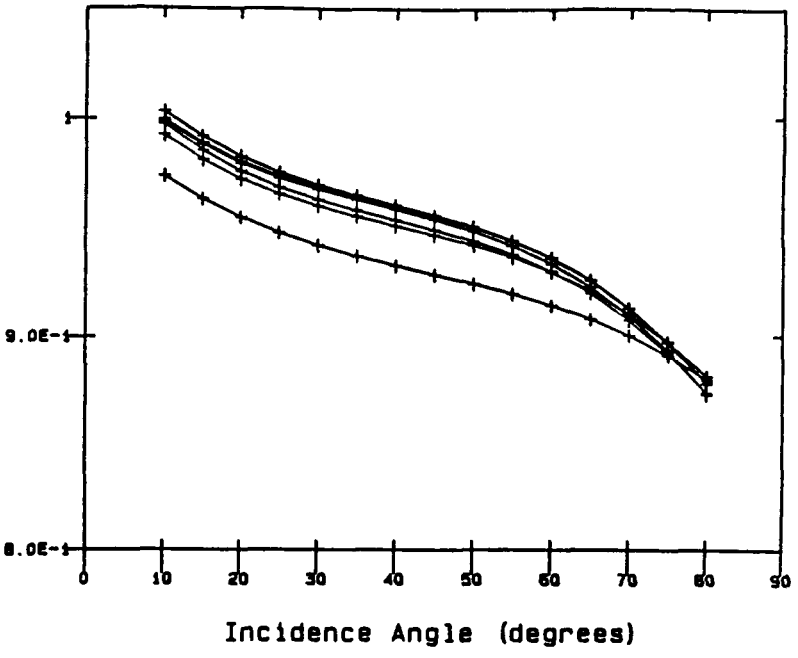

Figure 3. Panel OSC #2 reflectance factors.

A comparison between painted $BaSO_4$ panels for a wavelength of 450 nm is shown in Figure 4. At λ = 450 nm panels #2 and #3 are essentially identical. However, #2 has a higher reflectance than #3 at low incidence angles ($\theta \leq 30$ degrees) and lower reflectance at the high angles. The BRFs are greater than 0.95. Reflectance factors for panel #1 differ considerably from the other two. They are higher at low angles and decrease rapidly with increasing incident angles. For other wavelengths, the trend is the same.

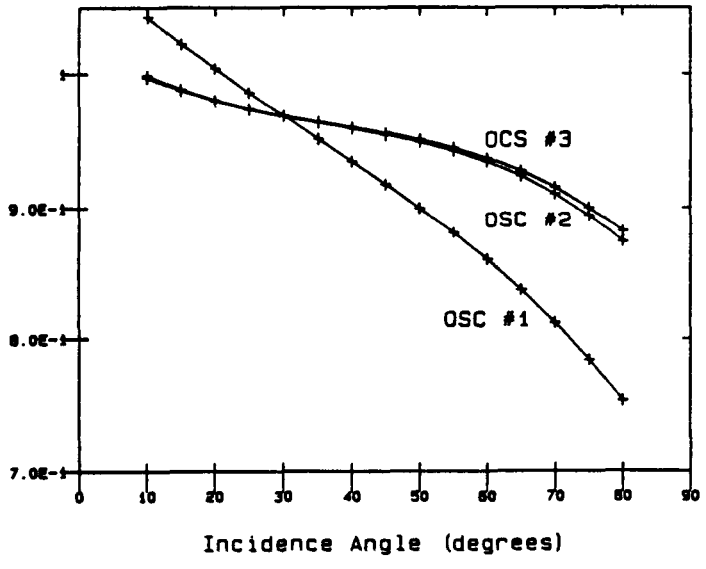

Figure 4. Reflectance factors at 450 nm.

Although the panels were painted by the same person using the same procedure, reflectance differences are observable. This emphasizes the need for meticulous care in the construction of the panels and demonstrates the need for careful calibration if they are to be used as a reference for ground-based measurements.

5. COMPARISON BETWEEN THE FIELD AND LABORATORY CALIBRATIONS

5.1. Summary of the field method[1]

The evaluation of $R(0^o; \theta)$ in the field required a halon reflectance standard of sufficient size (approximately that of the field standards) and a goniometer to position the reference panel at a known incidence angle to the sun. The measurements were recorded with a MMR which simulated the seven TM bands. The incidence angles ranged from 15 to 75 degrees in steps of 10 degrees. As the solar irradiance changed during the course of the measurements, the data-taking sequence was repeated immediately after completing the 75 degrees measurement but in reverse order. Then, the average of the two readings at each angle were used, minimizing the effect of the earth's rotation.

Because we were interested in directional quantities, we wanted only the direct solar beam. Thus, we needed to subtract the diffuse sky radiation from the total. This was done using a flat panel on a 3-m pole as parasol to alternatively shadow and expose the panel. Two diffuse measurements were made, averaged and subtracted from the sunlit measurement. The corrected data were processed as described above with the exception of fitting the incidence angle data to a third-order polynomial.

5.2 Differences between the laboratory and field conditions

There are three major differences between the laboratory calibration and the field calibration; they are the field of view (FOV) of the radiometers, the source, and the radiometer bandpass. In order to compare the results, the data from one experiment must be modified to correct for the differences.

The size of the laboratory, the geometry, and the size of the halon reference in the laboratory limit the FOV of the radiometers to about one degree in order to minimize any out-of-field contribution. In the field a 15 degree FOV is normally used to average over surface irregularities of the target. To compensate for this difference, the laboratory results were integrated over the field-radiometer field of view. The main effect was to smooth the reflectance factor curve and lower the value at large incidence angles.

The lamp source is quite different from the sun in several respects. The lamp is a finite distance from the panel providing a diverging beam whereas the sun gives a parallel beam. Hence, in the laboratory, the illumination of the panel over the FOV of the radiometer is not constant. We have calculated the effect numerically using a piecewise linear approximation to the FOV. This effect is dependent on both incidence and view angle. The effective temperature of the sun and the lamp are quite different. This results in an effective shift in the center wavelength of the radiometer bandpasses. The magnitude of the shift is dependent on the bandpass of the filter. It is negligible for narrow filters and is about 6 nm for a 100 nm filter such as the SPOT HRV XS1 filter. The method described in reference 7 was used to calculate the effective center wavelengths. Figure 5 shows the normalized irradiance of the sun and a lamp and the normalized filter response for XS1.

The final consideration is the radiometers' central wavelengths. The laboratory radiometer does not match the field instruments. We fit the data for a given incidence angle with a 3rd order polynomial in wavelength and interpolated to the required field radiometer wavelengths.

5.3 Comparison

Comparing the reflectance factor data with only a correction for wavelength, the largest difference was 0.02 in reflectance. With corrections for the FOV and the finite source distance, the largest difference was 0.013 in reflectance. Figure 6 shows the reflectance factors from the two methods.

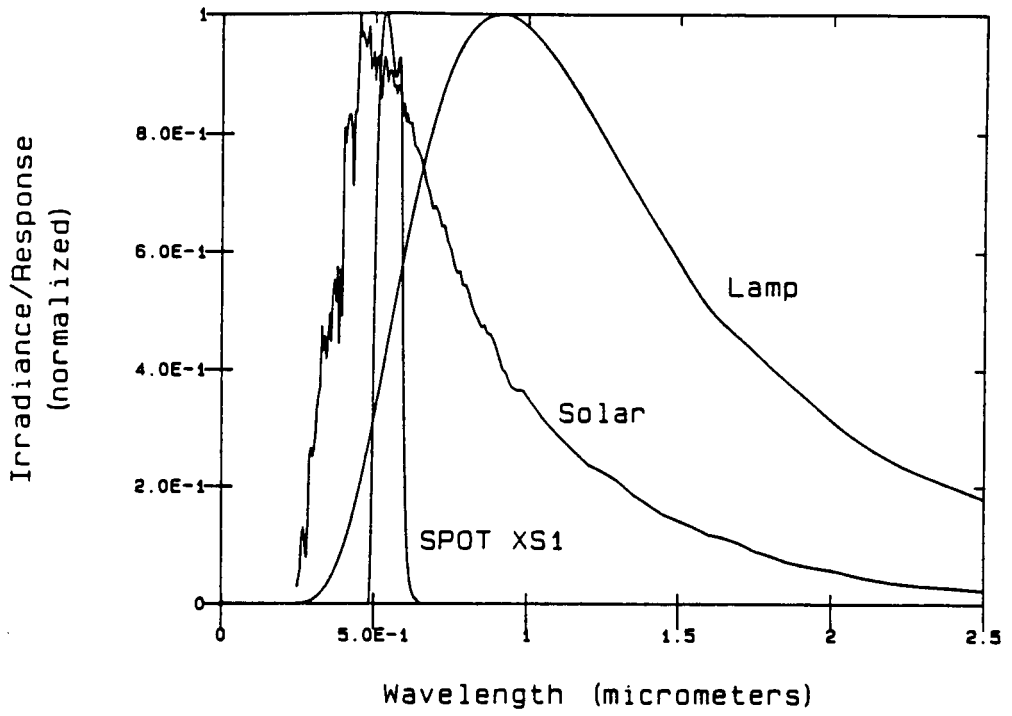

Figure 5. Normalized irradiance and filter response.

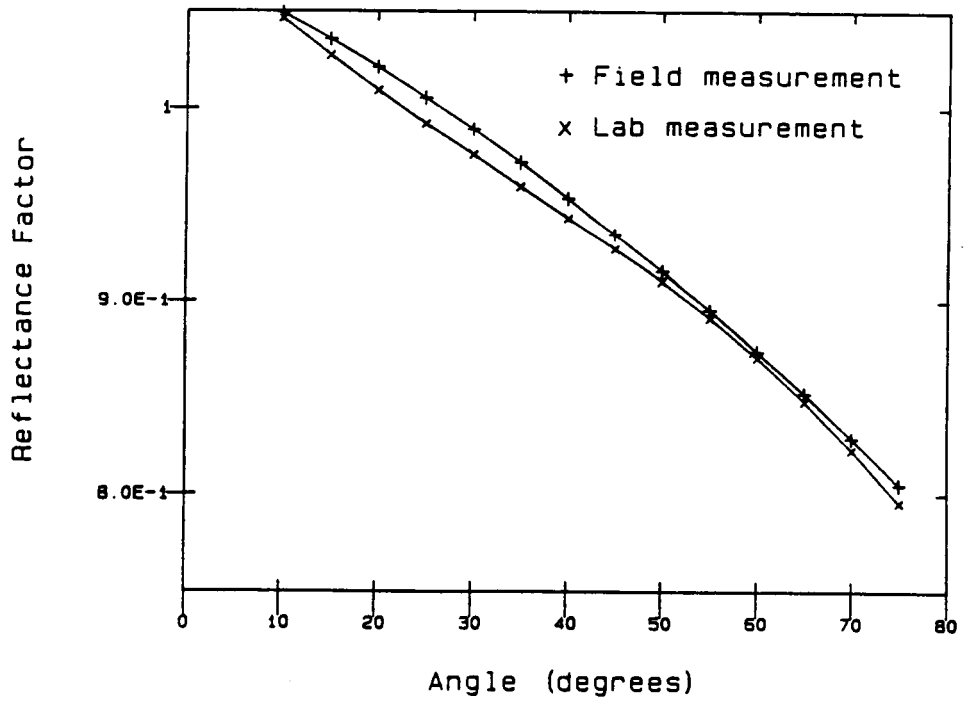

Figure 6. Reflectance factor.

6. CONCLUSIONS

A method and equipment have been described for the calibration of several field reflectance panels in terms of their directional reflectance factors. The results confirm the need for accurate calibration of any standard before field use.

The results of the measurements are very repeatable. They agree within 0.013 in reflectance with the results of an independent field method when corrections are made for geometry, wavelength and field of view differences. The automated equipment makes possible quick measurements, which facilitate the calibration of panels before and after important field experiments.

7. ACKNOWLEDGEMENTS

The work of authors at the Optical Sciences Center was supported under NASA grants NAGW-896 and NAG5-859.

8. REFERENCES

1. R. D. Jackson, S. M. Moran, P. N. Slater, and S. F. Biggar, "Field calibration of reference reflectance panels," Remote Sens. Environ. (22), 145-158 (1987).

2. B. L. Markham and F. M. Wood, "Radiometric calibration of the reflective bands of NS001 thematic mapper simulator (TMS) and modular multispectral radiometers (MMR)," Presented at the 1988 SPIE Technical Symposium, April 4-8, 1988 Orlando, Florida, SPIE this issue (1988).

3. V. R. Weidner, J. J. Hsia and B. Adams, "Laboratory intercomparison study of pressed polytetrafluoroethylene powder reflectance standards," Appl. Opt. 24(14), 2225-2230 (1985).

4. J. J. Hsia and V. R. Weidner, "NBS 45°/normal reflectometer for absolute reflectance factors," Metrologia 17, 97-102 (1981).

5. V. R. Weidner and J. J. Hsia, "Reflection properties of pressed polytetrafluoroethylene powder," J. Opt. Soc. of Am. 71(7), 856-861 (1981).

6. B. R. Robinson and J. J. Biehl, "Calibration procedures for measurement of reflectance factor in remote sensing field research," Proc. Soc. Photo-Opt. Instrum. Eng. (196), 16-26 (1979)

7. J. M. Palmer and M. G. Tomasko, "Broadband radiometry with spectrally selective detectors," Opt. Let. 5(5), 208-210 (1980).

APPENDIX 3.

Radiometric calibration requirements and atmospheric correction

Philip N. Slater
University of Arizona, Optical Sciences Center, Tucson, Arizona 85721

ABSTRACT

The need for independent, redundant absolute radiometric calibration methods is discussed with reference to the Thematic Mapper. Uncertainty requirements for absolute calibration of between 0.5% and 4% are defined based on the accuracy of reflectance retrievals at an agricultural site. It is shown that even very approximate atmospheric corrections can reduce the error in reflectance retrieval to 0.02 over the reflectance range 0 to 0.4.

1. INTRODUCTION

Absolute radiometric calibration provides the relationship between the digital counts recorded by a sensor and the spectral radiance at its entrance pupil. With correction for the atmosphere, it allows surface radiances, averaged over the sensor's bandpasses, to be determined. A knowledge of surface radiance is needed to determine, for example, energy balance relationships, retrieve ground reflectances, and map ocean chlorophyll concentrations. An accurate knowledge of the absolute calibration of sensors over their lifetimes allows data collected by different sensors at different times to be compared. An historical record of changes in sensor response is crucial to the success of long-term global science studies.

In this paper the need for redundant independent radiometric calibration procedures and the requirements for the accuracy of absolute calibration are discussed based on the analysis of results from calibration and reflectance retrieval measurements made at White Sands Missile Range, New Mexico, and Maricopa Agricultural Center, Arizona, respectively. Finally it is shown that approximate estimates for atmospheric correction can be effective in reflectance retrieval.

2. THE NEED FOR REDUNDANT CALIBRATION METHODS

There are three reasons, listed below, to use as many independent methods as possible for the absolute radiometric calibration of remote sensing systems. To illustrate these reasons, reference is made to Figure 1 from Slater et al.,[1] where the calibration of the Landsat 5 Thematic Mapper (TM) at White Sands, New Mexico, was made by reflectance- and radiance-based methods, referred to as CODE and HELI in the figure. These are also compared to the preflight calibration (PRE) and the internal calibrator (IC) results for that date.

1. No single absolute calibration method can be guaranteed to be free of systematic error. The agreement between precise independent methods to within their precisions provides the only way to confidently associate an uncertainty with an absolute calibration. For example, the good agreement between the three independent in-flight methods, shown in Figure 1, particularly in the first three TM bands, indicates that an absolute uncertainty within $\pm$ 5% has been attained.

2. The identification of a difference between two or more independent methods may help diagnose a change in the condition of the sensor. For example, in Figure 1 the results in general show that TM was more sensitive during preflight than in flight and that the internal calibrator results correspond to an instrument of greater sensitivity than the reflectance- and radiance-based results would indicate. Two conclusions can be drawn: first, the sensitivity of the TM has decreased since the preflight measurements, and second, part of the decrease appears to be due to a decrease in the reflectance of the scan mirror and image-forming optics and part to a loss in sensitivity of the filter-detector-electronics.

3. An analysis of the differences between two precise methods may expose an inadequacy or error in one of the methods which then may be corrected to improve the accuracy of future calibrations and measurements. For example, in Figure 1, the band 4 result for the reflectance-based method (CODE) is lower than any of the other results in that band, whereas in the other bands it is of intermediate value. This gave rise to a re-examination of the reflectance-based method in band 4 and the realization that the procedure followed resulted in an overcorrection for water vapor.[2] With a recalculation of water vapor absorption, the result in band 4 more closely matches the helicopter result, providing a more accurate method both for calibration and reflectance retrieval in band 4.

It is to be hoped that adequate resources will be available for the development and use of multiple radiometric calibration methods for future remote sensing systems. In addition to radiometric calibration and dynamic, micro-image performance characterization preflight, the use of a solar diffuser, lunar observations and earth surface reference site observations should be incorporated for in-flight calibration purposes.

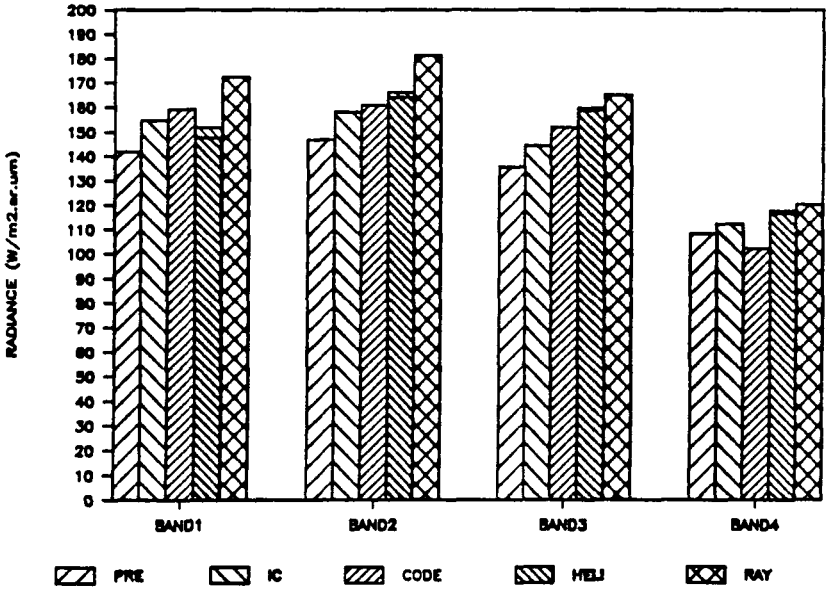

Figure 1. Comparison between the preflight (PRE) calibration of TM and the calibration results at White Sands on October 24, 1984, from the internal calibrator (IC), and reflectance- and radiance-based methods (CODE and HELI). The tips at the tops of the HELI bars are additions to account for the atmosphere above the helicopter. The calibration based on a Rayleigh atmosphere and ground reflectance measurements is shown as RAY.

3. REQUIREMENTS FOR ACCURATE ABSOLUTE CALIBRATION

It is neither difficult nor costly to provide the in-flight radiometric calibration of a multispectral sensor in an absolute sense at the ± 10% uncertainty level. To lower the uncertainty to the ± 3% level, however, is difficult and costly. To reduce it to the ± 1% level is unlikely at present, except for special cases.[3] Unfortunately, with the exception of the oceanography community, scientists in the earth surface disciplines have not developed requirements for uncertainty in absolute radiometric calibration. It is because of the close association of high cost with low uncertainty in calibration and the lack of well-justified requirements that the following study was conducted.

The starting point is the results, shown in Figures 2 and 3, of experiments conducted to determine the accuracy of a reflectance retrieval method.[4] Figure 2 shows the results of

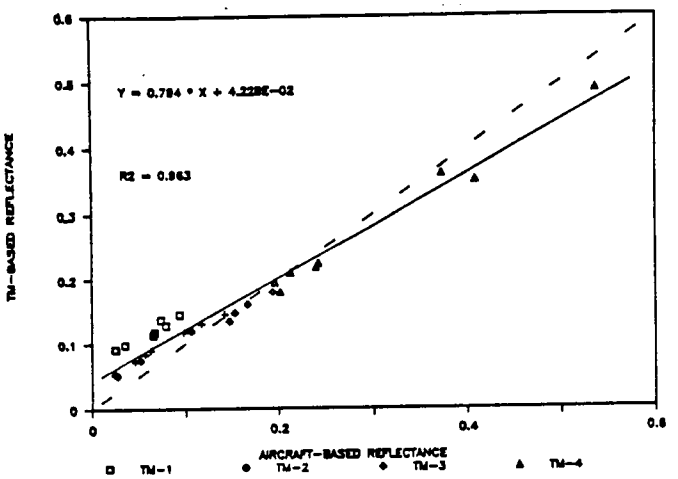

Figure 2. TM-based reflectances without atmospheric correction compared to reflectances obtained from low altitude aircraft measurements conducted nearly simultaneously with the TM image acquisitions.

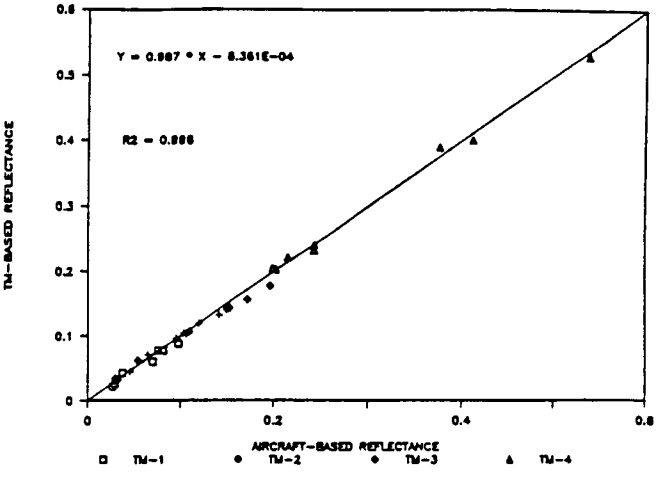

Figure 3. Same as Figure 2 but with atmospheric corrections based on the use of a radiative transfer code that used measured optical depths as inputs.

measurements made at Maricopa Agricultural Center (MAC) in Arizona on four days during a 16-month period, simultaneously with TM image acquisitions. In Figure 2, ground reflectances as determined by absolutely calibrated TM data are compared to ground reflectances as determined by an aircraft radiometer 150 m above the ground. The dashed line is the 1:1 line upon which all points should fall in the absence of an atmosphere. As expected, the low-reflectance band 1 TM-derived data show a substantial departure above the 1:1 line due to atmospheric path radiance, and at high reflectances atmospheric absorption brings the points below the line. Figure 3 shows the results after atmospheric correction where the atmospheric measurements and a radiative transfer code are the same as those used for calibration purposes at White Sands.[1,5] The much closer fit to the 1:1 line in Figure 3 compared to Figure 2 is obvious, and the equations on the graph provide quantitative evidence of this. Statistical analysis shows that the 1σ deviation of the reflectance values from the 1:1 line in Figure 3 is $\pm$ 0.008 and that this is fairly constant over the reflectance range 0.02 to 0.58.

It should be noted that this result is for uniform areas which were visually selected and registered with great care and for which any positional mismatch between the TM and aircraft samples gives rise to negligible error in the results. When several nonuniform entire fields at MAC were analyzed in this way, without the benefit of visual selection, the departure from the 1:1 line was 0.022 (1σ). No attempt was made to correct for the adjacency effect (atmospheric crosstalk) or sensor errors (the computer compatible tape images used were uncorrected for detector-to-detector variations within a band, the band average absolute calibration being used in all cases).

Based on the results shown in Figure 3, it appears that ground reflectances can be retrieved from absolutely calibrated, atmospherically corrected TM data to an accuracy of $\pm$ 0.01 over the reflectance range 0 to 0.6, at least for the first four TM bands. With this reflectance difference (delta rho) as input, the corresponding percentage change in digital counts or calibration was determined for the reflectance range 0.01 to 1.0 for an atmosphere with a visibility of 100 km, typical of the conditions for the MAC measurements. The results are shown in Figure 4, which includes all TM bands in the solar-reflective spectrum. With an intermediate reflectance of 0.25, the TM calibration error which introduces an error of 0.01 in the retrieval of that reflectance lies between 3% and 4% depending on the band. Note that the range in errors is introduced by the different dynamic ranges of the bands, band 1 having the shortest dynamic range, the greatest radiometric sensitivity, and therefore the least tolerance to calibration error for reflectance retrieval purposes.

Based on this analysis for TM band 1, the tolerance on calibration error is 3% for a reflectance of 0.25 to be retrieved with an error no greater than 0.01. On a root sum square basis, the error introduced in ground reflectance retrieval at 0.25 is negligible if the calibration uncertainty is about ± 1%. As the reflectance decreases below 0.25, according to Figure 4 the tolerance on calibration accuracy loosens. For example, at a reflectance of 0.05 it falls between 7% and 15%, but note that the reflectance error is still 0.01, which amounts to 20% of the reflectance value.

On the basis of results in Figure 4, at reflectance levels of 0.05, 0.25, and greater than 0.75, the calibration error to match the atmospherically corrected reflectance error is (averaged for the TM bands) 12%, 3.5%, and 1.5% respectively. For a negligible effect on reflectance retrieval accuracy, the calibration errors should be less than 4%, 1%, and 0.5% respectively. The difficulty in producing highly radiometric accurate data for snow field research purposes is obvious.

The limits beyond which it is futile to improve the accuracy of absolute calibration are dictated by natural variations, e.g. the mixed pixel condition, our ability to measure reflectance accurately at ground level, and our ability to make atmospheric corrections accurately, which is largely governed by our ability to accurately characterize aerosols.

4. EFFICACY OF SIMPLE ATMOSPHERIC CORRECTION

Figure 3 showed the results of applying atmospheric corrections based on atmospheric measurements made during the morning that the image of MAC was acquired by TM. It is of interest to determine how accurately a correction can be made that is based on a guess at the atmospheric conditions.

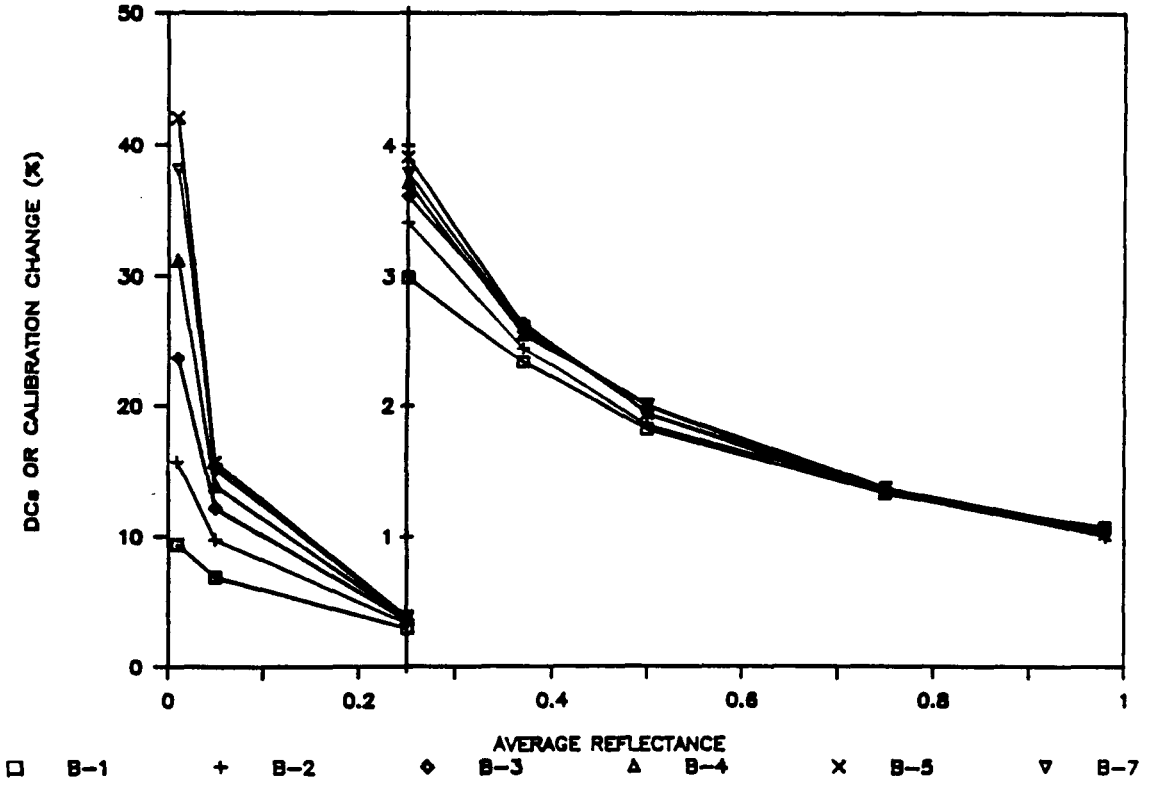

Figure 4. The percentage change in digital counts, or calibration, as a function of reflectance corresponding to a ground reflectance difference of 0.01 for a 100 km visibility atmosphere, a 45° solar zenith angle, and an aerosol complex refractive index of 1.54 - 0.01i.

The simplest example is that of a Rayleigh correction. Figure 5 shows the relationship between TM-based reflectances and ground reflectances for an atmosphere with a 100 km visibility. The error in the reflectance range for water, roughly 0 to 0.05, is high owing to atmospheric path radiance. Figure 6 supports the contention of Hovis[6] that a simple Rayleigh correction is very effective in this range although for the higher reflectances on the graph it is advisable to continue either to use the uncorrected values or, better, to take account of scattering due to aerosols.

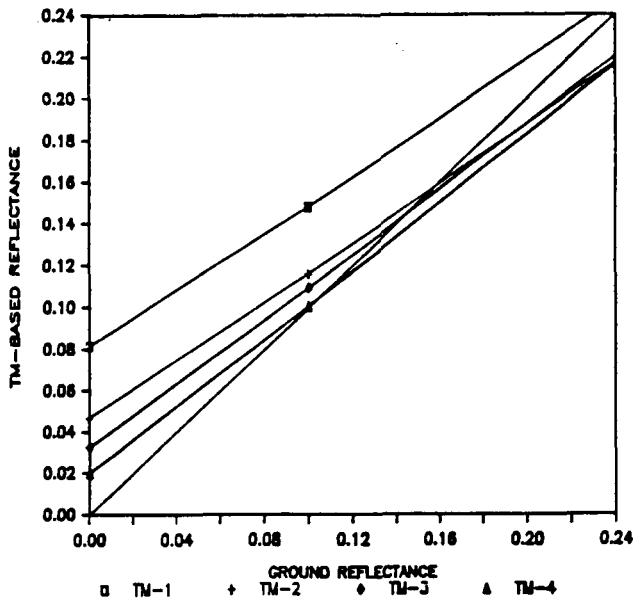

Figure 5. TM-based reflectance, uncorrected for the atmosphere, as a function of reflectance for a visibility of 100 km.

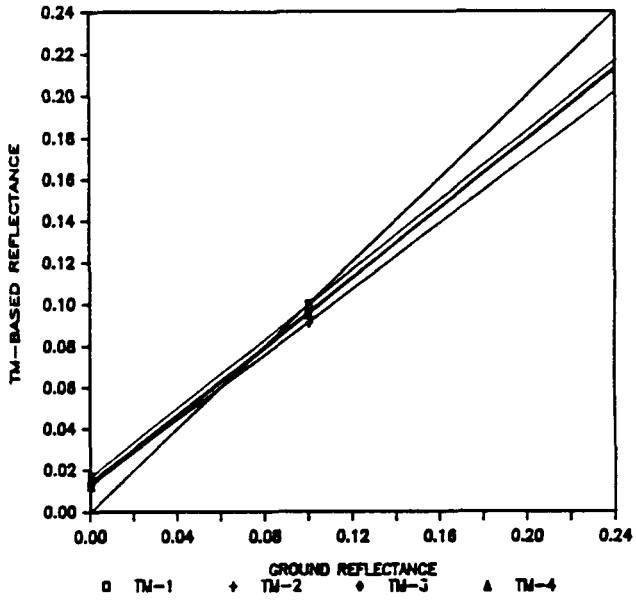

Figure 6. Same as Figure 5 but with a Rayleigh scattering correction.

Figure 7 shows the errors for TM-1 in making a simple atmospheric correction based on a guess at either the visibility or the aerosol optical depth. The actual atmosphere modeled has a visibility of 23 km and an optical depth for TM-1 of 0.452. As can be seen from the graph, errors in radiance of less than 5% at TM are introduced by optical depth estimates in error by as much as 50% over the reflectance range 0.1 to 1.0. The visibilities corresponding to $\pm$ 50% errors in the aerosol optical depth are 12.6 km and 44 km respectively. In other words, substantial errors in optical depth or visibility estimates may still allow quite accurate ground-radiance estimates to be made.

The above conclusion is also illustrated by Figure 8, which shows, for the three graphs starting in the top left of the figure, the reflectance differences introduced by three atmospheres having visibilities of 100, 23, and 10 km, as a function of ground reflectance. The three graphs below them on the left show the difference between TM and ground reflectance if corrections are made in all three cases assuming a 23 km visibility atmosphere. Obviously the actual 23 km visibility case has zero error while the 10 and 100 km actual visibility cases show errors within $\pm$ 0.02 in reflectance over the reflectance range 0 to 0.4, a considerable improvement over most of this range compared to the uncorrected cases.

Note that in the above examples, although the optical depths and visibilities were changed, the aerosol refractive index, or single scattering albedo, ω_o, was not. A change from 0 to 0.01 in the imaginary part of the index, corresponding to a change in ω_o from 1 to 0.89, can change the radiance in TM-1 by 8% for a reflectance of 0.25 and a 23 km visibility. This percentage is nearly constant over the reflectance range 0 to 0.5 and decreases with an increase in visibility. The

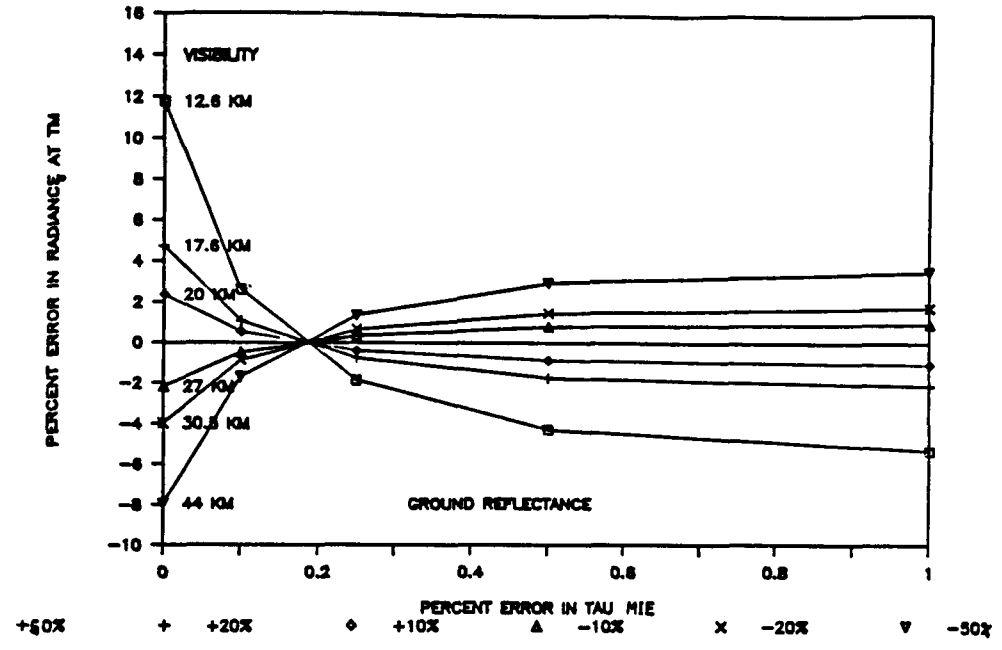

Figure 7. Percentage error in radiance correction for TM-1 as a function of ground reflectance. Departures from the 23 km visibility atmosphere correspond to differences in the 0.452 Mie optical depth of ± 10%, ± 20%, and ± 50%. The corresponding visibilities are shown on the left of the graph.

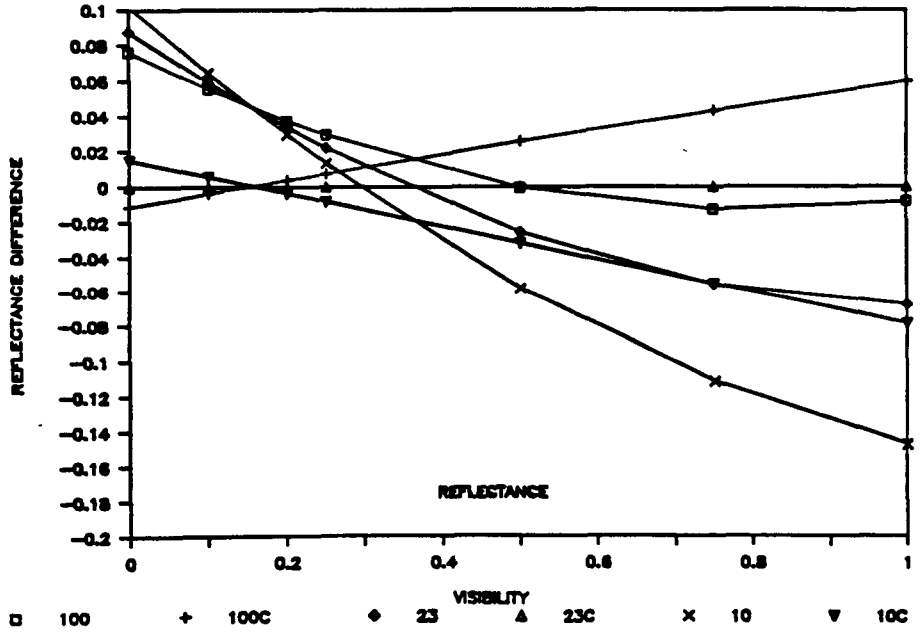

Figure 8. The three graphs starting in the upper left of the figure show the error introduced by three different atmospheres in the estimation of reflectances from satellite data. The three graphs below them on the left show the errors resulting when the same correction for a 23 km visibility atmosphere is applied to the results for all three atmospheres.

magnitude of the change emphasizes the need for accurate estimates of ω_o. However, in many rural areas ω_o is greater than 0.94 (imaginary part of index < 0.005). If the imaginary part of the index is chosen to be 0.0025, then the maximum uncertainty in the radiance at the sensor is ± 2% for 1 < ω_o < 0.94, a reflectance of 0.25, and a visibility of 23 km.

5. CONCLUSIONS

Several redundant and independent methods need to be used to provide confidence in estimates of uncertainty for absolute radiometric calibration. Comparisons between their results can be of use in determining the factors that change the sensitivity of a system and in revealing errors in the methods themselves.

The uncertainty in the calibration of future systems, based on the requirement for retrieving ground reflectances to an uncertainty of less than 0.01, varies with reflectance value. For a reflectance of 0.75 the requirement is 0.5% and this does not change significantly for reflectances up to 1.0. For a reflectance of 0.05 the requirement is 4% and this is more than adequate for lower reflectances. For reflectances between 0.05 and 0.75 the requirement lies between 4% and 0.5% depending on the reflectance, (see Figure 4).

Rough estimates of atmospheric conditions can, when used with radiative transfer programs that account for multiple scattering, provide effective atmospheric corrections for reflectance retrieval purposes. In fact almost any such atmospheric correction is better than none for low reflectance scenes. However, accurate and reliable ways to make atmospheric correction for any global location from satellite-acquired images need to be developed.

6. ACKNOWLEDGEMENTS

I wish to thank my coauthors in the three papers cited below for producing the results upon which this paper is based and for their valuable, critical comments. I also wish to acknowledge NASA grants NAG5-859 and NAGW-896 for their support.

7. REFERENCES

1. Slater, P. N., S. F. Biggar, R. G. Holm, R. D. Jackson, Y. Mao, M. S. Moran, J. M. Palmer, and B. Yuan, "Reflectance- and radiance-based methods for the in-flight absolute calibration of multispectral sensors," Rem. Sens. of Environ., 22:11-37 (1987).

2. Santer, R. P., University of Lille, France, communication to the author (1987).

3. Gordon, H. R., "Ocean color remote sensing: radiometric requirements," Proc. SPIE, 924, this issue (1988).

4. Holm, R. G., M. S. Moran, R. D. Jackson, P. N. Slater, B. Yuan, and S. F. Biggar, "Surface reflectance factor retrieval from Thematic Mapper data," Rem. Sens. of Environ., in press (1988).

5. Slater, P. N., S. F. Biggar, R. G. Holm, R. D. Jackson, Y. Mao, M. S. Moran, J. M. Palmer, and B. Yuan, "Absolute radiometric calibration of the Thematic Mapper," Proc. SPIE 660, pp. 2-8, (1986).

6. Hovis, W.A., "Landsat-4 Thematic Mapper calibration and atmospheric correction," Landsat-4 Science Characterization Early Results. Vol. III Pt 2, pp. 411-420, (1985).